Tidal wave propagation along The Mekong deltaic coast

Phan, Hung Manh; Ye, Qinghua; Reniers, Ad J.H.M.; Stive, Marcel J.F.

DOI
10.1016/j.ecss.2019.01.026

Publication date
2019

Document Version
Final published version

Published in
Estuarine, Coastal and Shelf Science

Estuarine, Coastal and Shelf Science 220 (2019) 73–98

Contents lists available at ScienceDirect

Estuarine, Coastal and Shelf Science

journal homepage: www.elsevier.com/locate/ecss

Tidal wave propagation along The Mekong deltaic coast

Hung Manh Phan[a,c], Qinghua Ye[a,b], Ad J.H.M. Reniers[a], Marcel J.F. Stive[a,*]

[a] Hydraulic Engineering Department, Delft University of Technology, PO-box 5048, 2600, GA, Delft, the Netherlands
[b] Deltares, Unit Software Center, P.O. Box 177, 2600, MH, Delft, the Netherlands
[c] Institute of Coastal and Offshore Engineering, Ministry of Agriculture and Rural Development, 658 Vovankiet Boulevard, Hochiminh City, Viet Nam

ARTICLE INFO

Keywords:
Tidal wave propagation
Resonance
Standing wave
Radial tidal currents
Mekong deltaic coast

ABSTRACT

A two-dimensional, barotropic numerical model was employed to investigate the dynamics of tidal wave propagation in the South China Sea with a particular interest for its characteristics along the Mekong deltaic coast. The study indicates that tidal waves propagate from the Pacific Ocean into the South China Sea mainly through the Luzon Strait (LS), where the K_1 diurnal tide dominates due to a quarter wavelength resonance in this semi-enclosed basin, and that the incoming tidal waves from the Celebes open boundary play a more important role than those from the Andaman and Flores open boundaries. Previous studies have not explained why both adjacent seas including the South China Sea and the Gulf of Thailand are dominated by a diurnal tide, while a semidiurnal tide dominates along the eastern Mekong deltaic coast. By means of Green's law, continental shelf tidal resonance theory and standing wave theory, this study clarifies that the large amplified M_2 semidiurnal amplitude leading to a prevailing mixed semidiurnal tide is caused not only by the shoaling effect and the continental shelf oscillation resonance phenomenon but also by the position on the standing wave anti-node line. Moreover, the finding of radial tidal currents occurring along the southern Mekong estuarine coast has not been revealed in earlier studies. Based on a number of numerical, geometrically schematised experiments, we suggest that the interaction between the large amplified amplitude near the shoreline associated with the adjacent low amplitude band system, causing convex hydraulic gradients of tidal amplitude due to basin geometry as well as sloping topography, is the mechanism for developing these radial tidal current systems. The results reveal that wind monsoon climate could cause either damped or amplified tidal amplitudes around the Mekong deltaic coast of which approximately 2–3 cm is due to the changing atmospheric pressure, the tangential stress of wind over the water surface and wind enhanced bottom friction. Also, this study suggests that the tidal generating forces should be considered to achieve accurate model results depending on the geographical region of interest. Findings achieved from this study contribute to a deeper insight of tidal wave propagation from a deep ocean to a shallow flat basin similar to the South China Sea and its Mekong deltaic coast.

1. Introduction

Most delta areas are controlled by three main factors, i.e. sediment input, wave action and tidal action (Galloway and Hobday, 1983), while the relative importance of these factors may differ. The Mekong delta may historically be well classified as a tide-dominated delta but the more western parts seem to be rather wave-dominated. This is probably reflected in the classification of Davis and Hayes (1984) where the coastal Mekong delta is classified as a mixed-energy (tide-dominated) environment affected by the flow regime of the Mekong River and its sediment load, the tidal regimes of the South China Sea (SCS) and the Gulf of Thailand (GoT), coastal currents driven by dominated monsoon winds and the related wave conditions (Delta Alliance, 2011). While several studies of wave processes along the Mekong deltaic coast (MDC) were conducted (Xue et al., 2012; Hein et al., 2013; Tas, 2016), tidal characteristics on the Mekong shelf have hardly been studied. Because the Mekong delta shelf is a transitional region between the deep sea of SCS and the shallow sea of GoT, the behaviour of tidal wave propagation along the MDC is distinctive and complicated. Being one of the key factors in controlling morphological processes of the MDC, it is necessary to achieve good understanding of the principal mechanisms of tidal wave propagation on the Mekong deltaic shelf from the SCS and the GoT.

The Taiwan Strait in the North, the Luzon and Palawan Islands in the East and the GoT in the Southwest and Kalimantan in the South surround the SCS. Co-oscillating tides mainly controlled by tidal wave

* Corresponding author.
E-mail address: M.J.F.Stive@tudelft.nl (M.J.F. Stive).

https://doi.org/10.1016/j.ecss.2019.01.026
Received 4 May 2018; Received in revised form 26 January 2019; Accepted 30 January 2019
Available online 13 February 2019

propagation on the Pacific Ocean and the Indian Ocean influence tidal wave characteristic in the SCS. The Pacific Ocean tides spread into the SCS through the Luzon Strait and the Celebes Sea, whereas the Indian Ocean tides influence the SCS through the Andaman, Lombok and Flores Seas. However, previous studies did pay little attention to these open boundaries for the tidal wave system in the SCS as well as in the MDC.

Some earlier studies on tidal characteristic in SCS comprise evaluations of tidal harmonic constituents using observation stations by Yu (1984), using Topex/Poseidon (T/P) altimetry data by Yanagi et al. (1997) and/or using numerical models by Ye and Robinson (1983), Fang et al. (1999), Zu et al. (2008), Gao et al. (2015). Several studies have shown that tidal waves propagate into the SCS mainly through the LS, and that several amphidromic systems exist on their continental shelves (Yanagi et al., 1997; Ye and Robinson,1983 and Fang et al., 1999). Although there are numerous studies on tidal characteristics of the SCS, only a few studies considered the tidal wave evolution in the shallower Southern Vietnam continental shelf, including the MDC. At the mouths of the Mekong River, the maximum and mean tidal ranges are 3.8 m and 2.5 m, respectively (Saito et al., 2015). The average tide range decreases with distance upstream (Gagliano and McIntire, 1968). All studies found that the tide is mainly diurnal in the whole South China Sea even including the Sunda Shelf and the GoT, while semi-diurnal tides dominate mostly in the region of freshwater influence (ROFI) of the MDC between the Vung Tau and Tran De branches (Nguyen et al., 1998). Zu et al. (2008) suggested that the shoaling effect on the shallower continental shelf of the Mekong region is causing the M_2 tidal amplitude to increase to nearly 1 m. However, the K_1 diurnal tide is amplified less than the M_2 semi-diurnal tide with an amplitude of only some 0.75 m in the MDC (Fang et al., 1999) even though the tidal progressive wave in the SCS is dominated by the K_1 diurnal component. Therefore, the reason why the semidiurnal tide dominates the tidal wave system in the region of the Mekong river mouth has not been adequately explained to date.

In most previous numerical studies of hydrodynamics in the SCS and the MDC, a tidal open boundary forcing at Luzon Strait is often introduced to force tides in this region. The effect of tidal generating forces on the tidal wave system in the SCS as well as along the MDC has not been considered. The SCS is a semi enclosed shallow sea and its massive body of water is nearly 5 km in depth with a surface area of 3.5 million km^2. Therefore, the contribution of the gravitational forces to the tidal wave motion increases considerably and it is necessary to investigate to what extent tide generating forces (TGF) influence the tidal wave propagation in the SCS and whether the role of tide generating forces is important for the tidal wave propagation along the MDC.

Tides can also be affected by local wind and weather patterns. The wind driven contribution to flow and water level changes the tidal amplitude (Wijeratne et al., 2012). The monsoon winds in the SCS are caused by the influence of the trade winds and the seasonal change between the location of the earth and the sun. The East Asian monsoons cause strong seasonal climatic variations in the Mekong Delta (Hordoir et al., 2006). Winds are coming mostly from northeast directions in the winter monsoon season from November to April and southwest winds prevail during the summer monsoon. Annual wind speeds have been recorded from 1999 to 2008 by the Southern Regional Hydro-Meteorological Center (Unverricht et al., 2014) at Vung Tau station ranging from 7 to 9 m/s and in Bac Lieu from 6 to 8 m/s. Under stormy conditions wind speeds can reach 20–30 m/s (Institute of Strategy and Policy on natural resources and environment ISPONRE., 2009). The maximum wind stress occurs along the southeastern coast of Vietnam in both monsoon seasons (Unverricht et al., 2014). Although previous studies (eg. Wyrtki, 1961) agree that the circulation of the SCS is affected mostly by monsoon winds, these studies do not distinguish the different effects between the north east monsoon and the south west monsoon to tidal wave systems. Therefore, it is necessary to clarify the role of wind monsoon climate influencing the tidal wave propagation in the Mekong delta. The mechanisms of tidal wave propagation in the Mekong delta shelf are revealed with the aid of the high-resolution process based model Delft3D.

In this study, a large-scale model covering the domain of SCS is setup, with a special interest in the South Vietnam Sea, to gain fundamental insight into the mechanisms of the overall tidal wave propagation in the SCS with specific attention for the MDC. After verification of the model with regard to the co-tidal patterns and tidal current ellipses of the main tidal components, the residual currents and the geographical distribution of tidal types, a sensitivity analysis of the open boundaries is conducted. Effects of several factors including wind climate monsoon, tidal generating forces and river discharges are examined using numerical experiments of the tidal wave propagation.

2. Numerical model

2.1. Model set up

The depth-averaged tidal dynamics model for the whole SCS has been constructed using Delft3D-FLOW, which includes the shallow water equations, the continuity equations and the transport equations for conservative constituents (Lesser et al., 2004). The details of the numerical schemes can be found in the Delft3D-FLOW user's manual (Deltares, 2014). The current model ranges from 96°-126°E and from 8°S −24°N with flexible orthogonal mesh features with grid cell sizes of nearly 22 km near the offshore boundaries and gradually reducing to 4 km around the MDC as shown in Fig. 1. The finer grids are necessary to resolve the topography needed for an accurate simulation. A total of 8 primary tidal constituents (O_1, K_1, P_1, Q_1, M_2, S_2, K_2, N_2) derived from 15 years of Topex-Poseidon and Jason-1 satellite altimetry (Gerritsen et al., 2003) adjusted to GMT 7 + have been applied for tidal simulations at 8 main boundaries, viz. Taiwan Strait, Luzon Strait, Celebes Zee, Flores Zee, Sape Strait, Lombok Strait, Sunda Strait and Andaman Zee.

The bathymetry data shown in Fig. 1 are obtained from the General Bathymetric Chart of the Oceans (GEBCO) bathymetry database (IOC, IHO, and BODC, 2003) with 30 arc-second grid resolution. Higher resolution bathymetry data along MDC are obtained from a bathymetry survey of the MDC in 2009 and 2010 in the context of a Vietnam Government project (SIWRR., 2010). The Manning bed friction coeffic ients selected after model calibration are 0.026 $m^{-1/3}s$ globally with some local values of n = 0.015 $m^{-1/3}s$ on the Vietnamese shelf and a value of n = 0.5 $m^{-1/3}s$ across the archipelagos separating the Sulu Sea from the SCS and the Celebes Sea, accounting for the effect of partly unresolved islands and underwater ridges. As the model domain covers a large area and the water depth of several sections is relatively deep, the TGF are included in this model and calculated including the equilibrium tide and the earth tide. In the model, the TGF of 10 tidal constituents (M_2, S_2, N_2, K_2, K_1, O_1, P_1, Q_1, MF, and MM) are considered. The six branches of the Mekong River are included as river boundaries with hourly discharges. The value for the horizontal eddy viscosity that is employed as a calibration parameter of Delft3D Flow depends on the flow and the grid size used in the simulation. Because of the large area with grid sizes of kilometers, the horizontal eddy viscosity is specified at 250 m^2/s (Gerritsen et al., 2003). For the shallow flat areas in the domain of the MDC, the process of drying and wetting is considered in this numerical model (Stelling and Kester, 1994). Computational grids are labelled either wet or dry by evaluating the total water depth at a grid cell or cell boundary with a threshold depth δ (in this study $\delta = 0.01$m). The model was set up with zero initial conditions. The time step of the simulation is 3 min. The first seven days are applied as a spin-up period and neglected in the analysis.

2.2. Model results validation

The simulation is carried out for the whole year of 2014 using a time

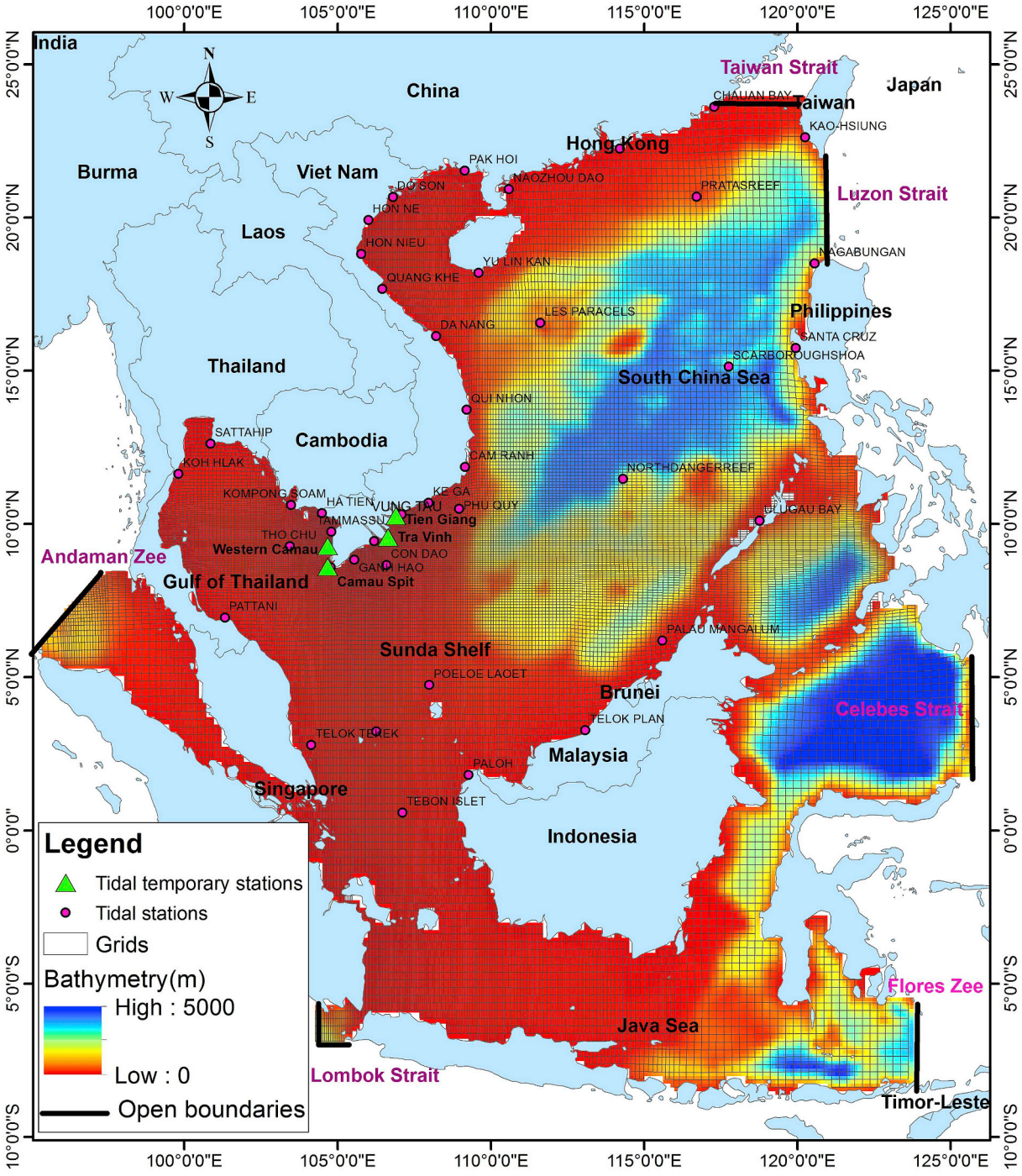

Fig. 1. Bathymetry, model setup and location of tidal data stations.

step of 3 min at zero initial conditions. In the whole SCS, along the MDC on the southern Vietnam shelf, 41 tidal stations were selected for model verification. Practical error measures for a tidal constituent k are the summed vector difference and root mean square error over selected observations:

$$SVDk = \sum_{s=1}^{s=S\,\max} VD_{k,s}$$

$$\mathrm{VD_{k,s}} = \sqrt{(A_{c,k}cosG_{c,k} - A_{o,k}cosG_{o,k})^2 + (A_{c,k}sinG_{c,k} - A_{o,k}sinG_{o,k})^2}$$

Where $A_{c,k}$, $G_{c,k}$, $A_{o,k}$, $G_{o,k}$ are the computed and observed astronomical amplitude and phase of tidal constituent k at stations s.

The RMSE of the complex amplitude is. $\sqrt{\frac{1}{2N}\sum_{i=1}^{N}|A_{Si} - A_{Oi}|^2}$ Where N is the number of the observation stations; A_{Si} and A_{Oi} are the model simulated and observed amplitude at station i, respectively.

Computed astronomical amplitudes and phases are analysed by a tidal harmonic analysis program called Delft3D-TIDE tool. The astronomical tide observed in oceans and seas is directly or indirectly the result of gravitational forces acting between the sun, moon, and earth. The influence of other celestial bodies on a yearly time-scale is negligibly small. The observed tidal motion can be described in terms of a series of simple harmonic constituent motions, each with their own characteristic frequency (angular velocity). The amplitudes A and phases G of the constituents vary with the positions where the tide is observed. The general formula for the astronomical tide is:

Table 1
Comparison of the harmonic constants between observed and calculated results for M_2 constituent.

No	Station name	LONG	LAT	M2						
				Observation		Calculation		dH	dG	VD
				Amp A (cm)	Phase G (deg.)	Amp A (cm)	Phase G (deg.)	(cm)	(deg.)	(cm)
1	YU LIN KAN	109.606	18.19	20.3	303	21.6	312.0	−1.26	−9.0	3.5
2	PAK HOI	109.145	21.529	38.3	192	42.6	201.3	−4.28	−9.3	7.8
3	DO SON	106.808	20.667	5.4	76	9.2	81.0	−3.79	−5.0	3.8
4	HON NE	106.006	19.918	26.4	36	31.2	45.6	−4.81	−9.6	6.8
5	HON NIEU	105.777	18.81	30.3	31	35.3	40.1	−4.95	−9.1	7.2
6	QUANG KHE	106.464	17.671	17.6	41	23.0	39.4	−5.37	1.6	5.4
7	DA NANG	108.214	16.127	17.2	330.1	13.0	324.0	4.21	6.1	4.5
8	QUI NHON	109.212	13.732	17.3	321.1	10.3	316.7	6.96	4.4	7.0
9	CAM RANH	109.159	11.858	19.1	329.1	12.9	323.5	6.23	5.6	6.4
10	PHU QUY	108.967	10.497	18.9	345.6	21.1	336.2	−2.15	9.4	3.9
11	KE GA	107.969	10.689	36.4	23	37.9	24.5	−1.47	−1.5	1.8
12	VUNG TAU	107.086	10.305	79.2	65.1	70.9	68.9	8.35	−3.8	9.7
13	CON DAO	106.593	8.656	80	81.1	75.0	90.7	5.00	−9.6	13.9
14	MY THANH	106.193	9.432	95	86.39	90.2	92.0	4.80	−5.6	10.3
15	GANH HAO	105.458	9.037	108	118	101.3	124.3	6.67	−6.3	13.3
16	CA MAU	104.78	8.58	15	97	10.7	101.0	4.29	−4.0	4.4
17	Tammassu	104.796	9.006	10.5	135	15.3	143.0	−4.83	−8.0	5.1
18	HA TIEN	104.494	10.35	9.8	119	12.5	127.1	−2.70	−8.1	3.1
19	THO CHU	103.444	9.272	3	23	6.3	22.4	−3.30	0.6	3.3
20	KOMPONG SOAM	103.483	10.62	11.3	35	15.3	53.7	−4.00	−18.7	5.9
21	SATTAHIP	100.859	12.622	20.7	163.1	12.6	171.3	8.06	−8.2	8.4
22	KOH HLAK	99.245	10.427	5.1	168.4	7.2	159.1	−2.06	9.3	2.3
23	PATTANI	101.325	6.943	21	312.1	20.5	310.2	0.50	1.9	0.9
24	TELOK TEKEK	104.144	2.785	52.9	274.6	40.1	269.1	12.77	5.5	13.5
25	TEBON ISLET	107.118	0.582	5	204.8	8.6	192.1	−3.56	12.7	3.8
26	SELAT PENINTING	106.263	3.225	13	267.1	9.6	258.8	3.42	8.3	3.8
27	POELOE LAOET	107.992	4.741	9	85	16.4	79.5	−7.37	5.5	7.5
28	PALOH	109.275	1.807	60	106.4	40.8	99.8	19.20	6.6	20.0
29	TELOK PLAN	113.085	3.264	20.1	54.1	28.5	48.2	−8.44	5.9	8.8
30	PALAU MANGALUM	115.592	6.198	23.5	320.1	24.4	311.3	−0.93	8.8	3.8
31	ULUGAU BAY	118.77	10.104	20	304.1	17.0	291.3	3.00	12.8	5.1
32	SANTA CRUZ	119.948	15.739	11.7	263.1	15.5	272.8	−3.80	−9.7	4.4
33	NAGABUNGAN	120.56	18.498	7.6	191.8	9.6	210.8	−2.04	−19.0	3.5
34	KAO-HSIUNG	120.252	22.618	15.9	236.7	19.4	243.9	−3.45	−7.2	4.1
35	CHAUAN BAY	117.292	23.609	75.3	14.3	55.1	22.2	20.20	−7.9	22.1
36	HONGKONG	114.207	22.249	40.4	267.9	30.2	273.4	10.19	−5.5	10.7
37	NAOZHOU DAO	110.589	20.927	78.8	313.1	84.7	330.4	−5.94	−17.3	25.3
38	NORTHDANGERREEF	114.31	11.469	20	298.1	19.2	303.4	0.75	−5.3	2.0
39	SCARBOROUGHSHOA	117.765	15.137	20	305.1	15.9	290.0	4.06	15.1	6.2
40	LES PARACELS	111.617	16.557	16.8	297	18.3	298.3	−1.55	−1.3	1.6
41	PRATASREEF	116.716	20.678	14.2	257.5	11.8	250.5	2.44	7.0	2.9
Average SVD										7.0
RMSE								6.7	8.8	

$$H(t) = A_0 + \sum_{i=1}^{k} A_i F_i \cos\left(w_i t + (V_0 + u)_i - G_i\right)$$

Where: H(t): water level at time t; A0: mean water level over a certain period; K: number of relevant constituents; I: index of a constituent; Ai: local tidal amplitude of a constituent; Fi: nodal amplitude factor; Wi: angular velocity; $(V0 + u)_i$: astronomical argument; Gi: improved kappa number (=local phase lag)

The Delft3D-TIDE tool is formulated in terms of k relevant constituents, a total of (2k +1) unknowns A0, Ai and Gi must be determined (or (2k +2) unknowns, if an additional term Bt is included). As a result of non-resolvable very long period constituents or non-astronomical phenomena, the mean water level may vary slowly. To take account of such motions, if present, the B_t term is included in the general formula for the astronomical tide, representing a trend. This is realised by minimisation of the quantity: $\sum (W(t) - H(t))^2$ using a least-squares technique.

The harmonic constants of the water level from 41 observation stations (Fig. 1) are collected from the International Hydrographic Organization (IHO) tidal dataset, published data by Fang et al. (1999) and Zu et al. (2008), data from permanent stations of Vietnam Southern Regional Hydrometeorological Center as well as from the Global Tide Model. The Global Tide Model developed by the Technical University of Denmark is available on a 0.125 × 0.125° resolution grid for the major 10 constituents in the tidal spectra. The model is utilizing the latest 17 years of multi-mission measurements from TOPEX/Poseidon, Jason-1 and Jason-2 satellite altimetry. The computed and observed harmonic constants are listed together for comparison. The SVD and RMSE are generally small as shown in Table 1. Furthermore, other four temporary measurements stations along the MDC (Table A.2) collected from national projects of Vietnam government are employed for validation of tidal currents simulations (ICOE., 2011; ICOE., 2014; SIWRR., 2016).

3. Results

3.1. Cotidal charts

3.1.1. The semi-diurnal tides

The co-amplitude and co-phase lines of the semidiurnal tides in Fig. 2 are obtained from the calculated tidal harmonic components. The M_2 tide propagates mainly southwestward from the Pacific Ocean

through the Luzon Strait into the SCS as a progressive wave and a minor part of the M_2 tide turns northward into the Taiwan Strait (TS) as a Kelvin wave. During the propagation, a small branch of it propagates northwestwards into the Gulf of Tonkin, while its main part continues to propagate southwestwards. When the tidal wave reaches the area adjacent to the southwest of Vietnam, part of it turns into the GoT and another part spreads southwards to the Sunda Shelf. The results show that the M2 amplitude is generally small (0.18–0.19 m) in the central part of the SCS with a wave speed of nearly 160–180 m/s which can be valued from c = L/t, where L is the distance between two adjacent co-phase lines and t is time duration which wave travels between those two co-phase lines. Meanwhile, the amplitudes in areas including TS, the south of Guangdong around Leizhou Peninsula, the northwest coast of Kalimantan, the south of the Vietnam, and around the western and southern parts of the Malay Peninsula are more than 1m.

A nodal band can be observed along a line roughly corresponding to the axis of the GoT and spreading to the area between Singapore and the west of Kalimantan (Indonesia). The study area is close to the equator leading to a weak Coriolis force. The evidence of this phenomenon is the unusual clockwise amphidromic system of the semi-diurnal tide M_2 in the mouth of the Gulf of Thailand (Yanagi and Takao, 1998), as according to the theory it should have a counter-clockwise rotation in the northern hemisphere. The inertia period Ti ($=2\pi/f$, f; the Coriolis parameter $= 2\omega\sin\varphi$, ω; the angular velocity of the earth's

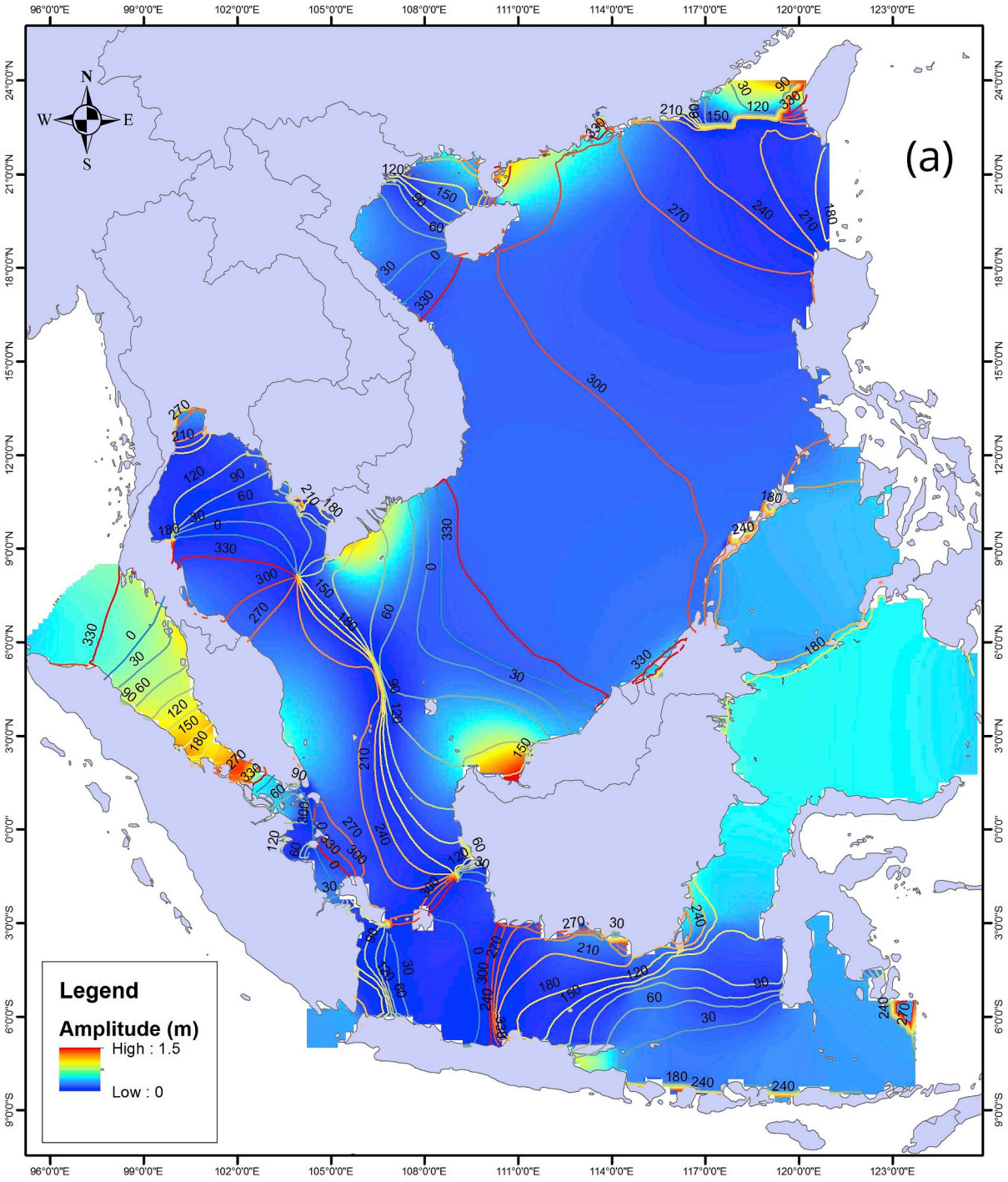

Fig. 2. Co-tidal charts of semi-diurnal M_2 (a) and diurnal K_1 (b).

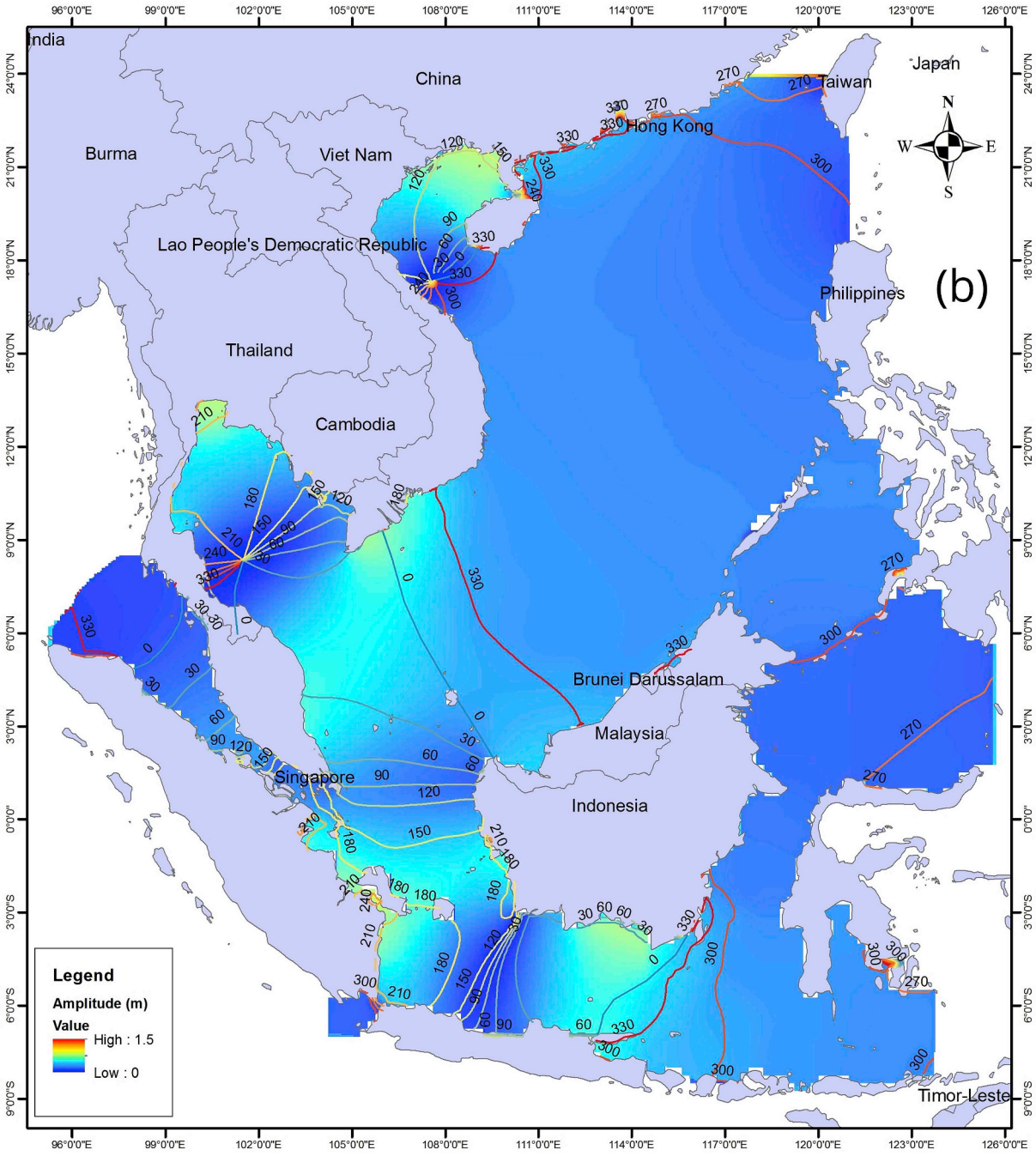

Fig. 2. (*continued*)

rotation, φ; the latitude = 7°N in this case) of the Sunda shelf is 98.5 h. The Rossby deformation length λ (=gH/f) of the shelf is 1580 km with the average depth of the Sunda shelf being roughly 100m. Semi-diurnal and diurnal tidal periods are therefore much shorter than the inertial period and the width of the Sunda shelf of approximately 950 km is narrower than the Rossby deformation length. These facts suggest that the Coriolis force on the Sunda shelf does not seriously affect the tidal phenomena. Therefore the condition is not favourable for a Kelvin wave tide to occur, especially looking at the pattern of the tidal wave propagation onto the Sunda shelf in the same phase.

The M_2 tide is amplified on the southern Vietnam shelf up to 1.1 m at the coastal zone of Baclieu province. When the M_2 tide from the deep SCS travels into shallower water in coastal southern Vietnam (CSV), the celerity will decrease which results in a concentration of energy and thus an increase in tidal amplitude called shoaling. The average water depth of the SCS is about 2500m and the continental shelf area of Southern Vietnam is about 100m. Green's law expresses the increase in amplitude as the wave shoals toward the coast:

$$A_s = \left[\frac{D_d}{D_s}\right]^{1/4} A_d \quad (1)$$

Where: A: the amplitude of tide.

D: the water depth

s, d: shallow (coastal zone) and deep water, respectively.

With an average amplitude of M_2 in SCS of nearly 0.18m, the average amplitude of M_2 in the CSV should be approximately 0.4m due to the shoaling effect from Eq (1). However, the average M_2 tide amplitude occurs to be about 0.9m–1.0m in this region, exceeding the amplitude value due to the shoaling effect. Therefore, this larger amplified M_2 amplitude is triggered by not only the shoaling effect but also by another effect viz. resonance. According to the theory of Clarke and Battisti (1981), continental shelf tidal resonance occurs when the shelf scale L is approximately equal to the shelf width:

$$L \approx g\alpha/(\omega^2 - f^2) \quad (2)$$

Where:

α: the shelf bottom slope based on Vietnam southern shelf bathymetry = 0.00067 (GEBCO).

ω: M_2 tidal frequency = 1.405×10^{-4} s^{-1},

f: the Coriolis parameter = $2\omega_e \sin ø = 0.228 \times 10^{-4}$ s^{-1}, ω_e: the angular velocity of the earth's rotation, ø: latitude = 9°N in this region.

The shelf scale L calculated by Eq (2) is nearly 340 km, which is roughly equal to the southern Vietnam shelf width of 350 km, hence the semidiurnal resonance effect of M_2 occurs. Therefore, the M_2 amplitude amplification up to 1.1 m at Baclieu Province's coast is not only due to the shoaling effect but also due to the continental shelf tidal resonance phenomenon. Both these phenomena cause a prevailing semidiurnal tide along the eastern MDC enclosed by diurnal tide in the SCS and GoT. The propagation of S_2 tide shown in Figure A1 is similar to that of M_2 tide, but the amplitude of S_2 is much smaller than that of M_2.

3.1.2. Diurnal tides

Like the M_2 tide, the K_1 tide mainly propagates into the SCS from the Pacific through the LS (Fig. 2). The rotation direction of the K1 tide in the GoT is opposite to that of the M_2 tide due to the particular M_2 tidal frequency as well as due to the influence of the Coriolis force on the K_1 tidal wave being larger than that on the M_2 tidal wave as a result of its longer period (Yanagi and Takao, 1998). Some areas with high K_1 amplitudes are located on the Gulf of Tonkin (about 0.7–0.9 m), in the northern part and the mouth of the GoT and at the south of the Kalimantan Strait (about 0.6 m). In contrast to the condition of the M_2 tide, the amplitude of K_1 is noticeably increased in the SCS basin (about 0.3–0.4m) after spreading from the Pacific (about 0.1–0.15m) through the LS. Therefore, it is suggested that the amplification of K_1 is caused by the resonance in the SCS. The natural oscillation period of the SCS is derived from the following equation for a semi-closed basin (Proudman, 1953):

$$T_i = \frac{4L_b}{(2\,i - 1)\sqrt{gH}} \quad (3)$$

Where i stands for the mode number, Lb (=2700 km) denotes the length of SCS from the Luzon Strait to the eastern Malaysian Peninsula, g (=9.81 ms^{-2}) is the gravitational acceleration and H (=1700m) represents the mean depth of the SCS. The natural oscillation period of the SCS is 23.2 h h close to the K_1 diurnal period of 23.9h. The resonance in the SCS is also found in the O_1 diurnal period of 25.8h (Figure A1).

Moreover, the resonance phenomenon also amplifies the diurnal tide significantly in the Gulf of Tokin and the GoT by. The inertial period *Ti* (=$2\pi/f$, *f*; the Coriolis parameter = $2\omega \sin\varphi$, ω; the angular velocity of the earth's rotation, φ; the latitude = 19.5°N in this case) of the Gulf of Tokin is 35.9 h. The Rossby deformation length λ (= gH/f) of the gulf is 455 km. Both semi-diurnal and diurnal tidal periods are much shorter than the inertial period and the width of the gulf is narrower than the Rossby deformation length in the Gulf of Tonkin. These facts suggest also that the Coriolis force in the Gulf of Tokin does not seriously affect the diurnal tidal phenomena. The length and mean depth of the Gulf of Tokin are approximately 520 km and 50 m, respectively. The natural oscillation periods along the Gulf of Tonkin calculated from Eq (3) is 26.1 h close to O_1 diurnal period of 25.8 h.

The GoT is situated in the southwestern part of the SCS and the length from the shelf edge to the head of the gulf, *L*, is about 1450 km; and its average depth, *H*, is about 55 m. Similarly, the natural oscillation periods along a semi-closed basin of the GoT from Eq. (3) are T_1 = 69.4 h, T_2 = 23.1 h, and T_3 = 13.9 h and nearly equal to the K_1 diurnal period. Although the diurnal tide controls both the Gulf of Tokin and the GoT, the O_1 diurnal tide and K_1 diurnal tide dominate in the Gulf of Tokin and the GoT, respectively.

3.2. Tidal currents field and residual currents

A common investigative tool for tidal currents is a plot of tidal current vectors. Over a tidal cycle, the current vectors typically trace out a tidal ellipse. Fig. 3c and d shows the simulated tidal ellipses of the M_2 and K_1 tidal constituents along the Southern Vietnam Coast. The tidal current ellipses of the M_2 tide indicate strong currents on the eastern coast of the Mekong Delta amounting to approximately 35–45 cm/s, while weak currents take place on the western coast. It can be clearly seen that large tidal currents occur in places with large tidal amplitudes.

Moreover, the tidal ellipses in the region off the Mekong River mouth are rectilinear and have a strong cross-shore component, which may be related to a standing wave. However, the tidal ellipses in the south of the Mekong River mouth are broader and have an alongshore component. This shape rather corresponds to a progressive wave. In contrast to the tidal current ellipses of the M2 tide, the tidal current ellipses of K_1 represent rather weak currents both on the eastern and western Mekong delta coast. In contrast, both tidal current ellipses of M_2 and K_1 show rather strong currents and rectilinear shapes on the Camau peninsula.

Tide-induced residual currents always play a key role in the oceanic processes, especially in the shallow coastal regions (Lee et al., 2011); the tide-induced residual current fields are also computed and shown in Fig. 3e. It can be found that the residual current increases mainly toward the southwest of the shallow MDC and is strongest along the Camau peninsula, amounting roughly to 10–15 cm/s. The finding of the tide-induced residual current with a direction from northeast to southwest along the eastern MDC from this numerical model is in accordance with previous geological studies (Nguyen et al., 2000; Ta et al., 2002; Unverricht et al., 2013). A part of the tidal currents continues to flow toward the southwest but the main part of those tidal currents are oriented toward the GoT with diminished magnitude. Based on the distribution of the residual currents combined with the tidal current ellipses of the M_2 semidiurnal tide a standing wave in the region off the Mekong and a corresponding progressive wave in the south of the Mekong River mouths are apparent.

On the other hand, according to tidal current fields in the flood tide and ebb tide from Fig. 3a and b, it seems that a radial tidal current field exists to the south of the Mekong river mouth and Baclieu is the focal point of the converging and diverging currents. This radial tidal current phenomenon also occurs at other places in the world, for instance at the Jiangsu coast in China, which has a larger strength of the radial tidal current velocities compared with the MDC. Su et al. (2015) showed that radial tidal currents in Jiangsu coast are controlled by the special local convergent tidal wave pattern from the meeting of the rotating tidal wave and the incident tidal wave. Furthermore, based on analyzing tidal current system, Yao (2015) suggested that the radial tidal currents are able to appear in a basin including the basin length larger than the width, a depth variation or an oblique tidal wave.

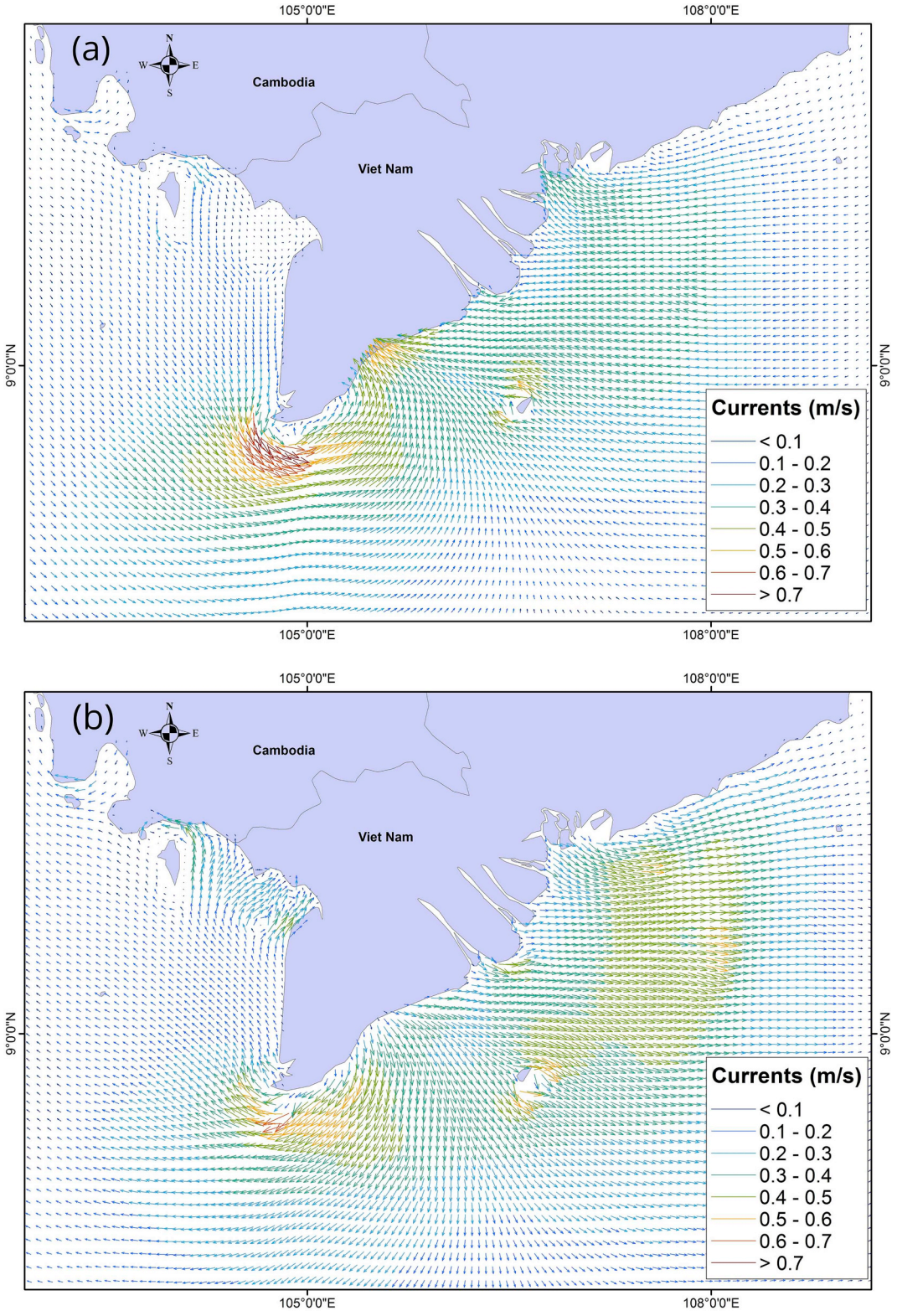

Fig. 3. Tidal currents in the flood tide (a), the ebb tide (b), the tidal current ellipses of M_2 (c), K_1 (d) and tidal-induced residual currents (e).

3.3. Geographical distribution of tidal characteristics

Classification of the type of tide is based on characteristic forms of a tide determined by the local relationship of the semidiurnal and diurnal tidal constituents. Tide types may be quantitatively classified (e.g., Defant, 1961) by the amplitude ratio (F ratio) of:

$$F = (K_1 + O_1) / (M_2 + S_2)$$

K_1, O_1, M_2, S_2 are the principal lunar diurnal constituents, the principal solar diurnal constituent, the principal lunar semidiurnal constituent and the principal solar semidiurnal constituent,

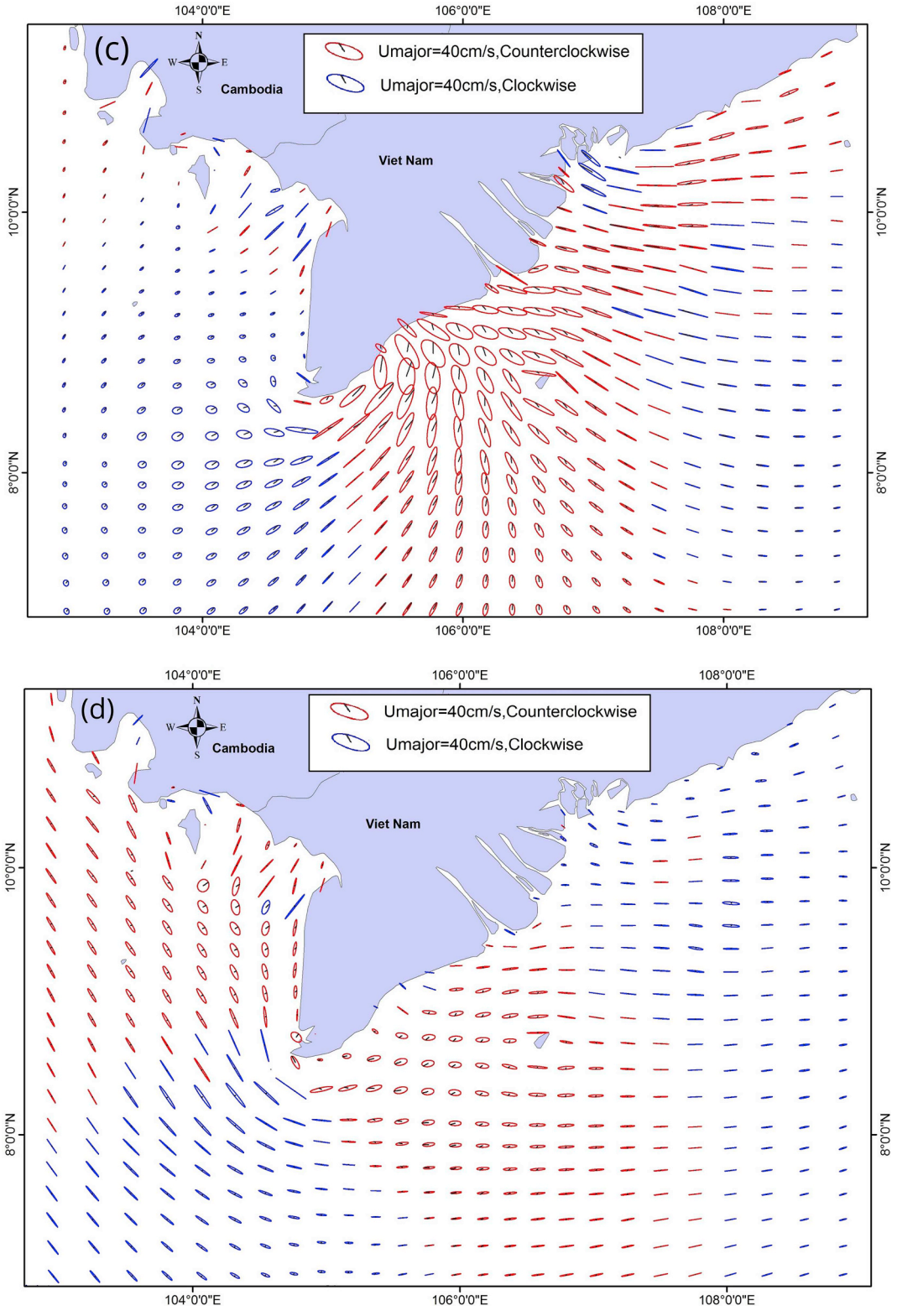

Fig. 3. (*continued*)

respectively. If the ratio is less than 0.25, the tide is classified as semidiurnal; if the ratio is from 0.25 to 1.5, the tide is classified as mixed, mainly semidiurnal; if the ratio is from 1.5 to 3.0, the tide is classified as mixed, mainly diurnal; if the ratio is greater than 3.0, the tide is classified as diurnal.

The results show that the tidal waves in the SCS are greatly affected by the depth and shape of the basins in which they propagate. The natural oscillation period of the various basins for the main tidal constituents are producing zones with predominantly diurnal tides and zones with predominantly semi-diurnal tides. Fig. 4 indicates that mixed diurnal tides dominate in the SCS, while there are some rare regions where a semidiurnal tide dominates due to the natural

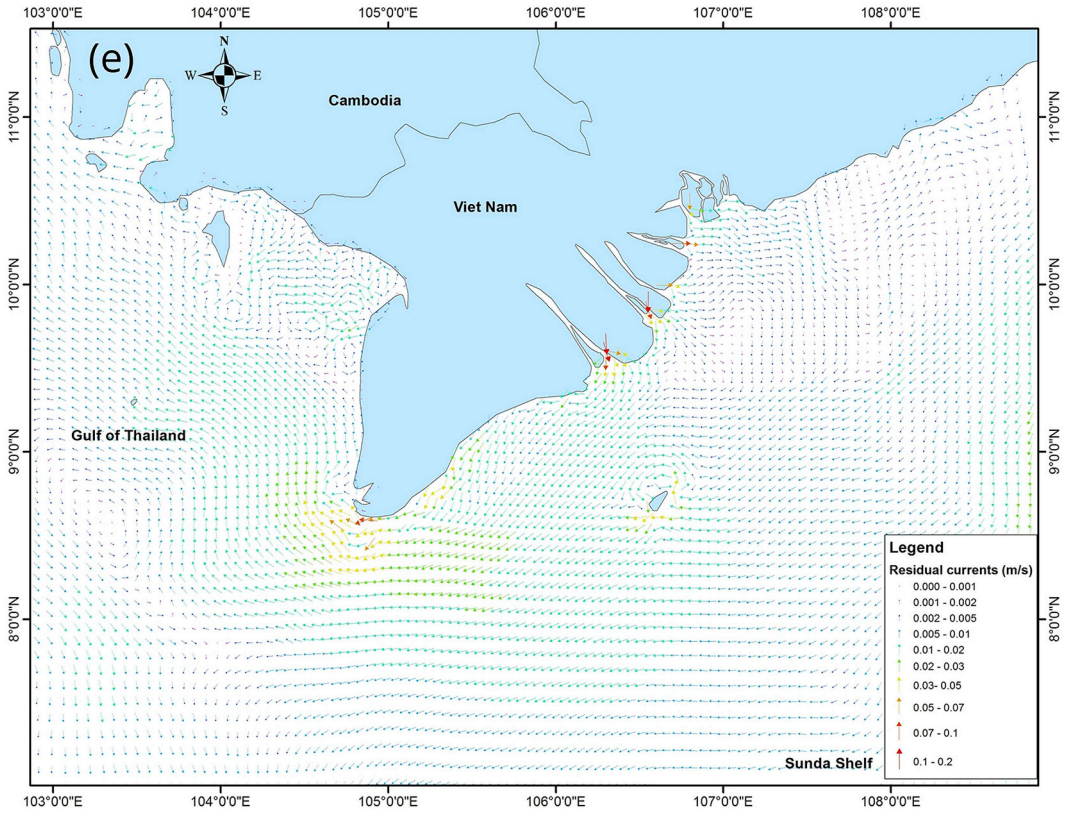

Fig. 3. (*continued*)

oscillating period of SCS close to the diurnal period. A pure prevailing diurnal tide is only found in the GoT, the Gulf of Tonkin, waters between Sumatra and Borneo and the south-west of Luzon Strait due to local conditions. These findings are in contrast with the results from Yanagi et al. (1997) claiming that a pure diurnal tide dominates in the whole SCS. Besides, this study improves the tidal classification on the western MDC by Wyrtki (1961). These authors propose that a mixed diurnal tide dominates on this coast, but in reality the tide is purely diurnal.

Fig. 4 shows that semi-diurnal tides dominate in the regions such as Malacca Strait connected directly to the Indian Ocean, Taiwan Strait linked to the East China Sea and South West in GoT. Mixed semi-diurnal tides exist in south of Guangdong, the northwest coast of Kalimantan, the southwest of Thailand and the continental shelf of the Mekong delta. All above regions are shallow continental shelves with concave coastlines, which are significant factors to increase the M_2 tidal semi-diurnal amplitude due to the natural oscillation period of these basins close to the semi-diurnal period.

3.4. Sensitivity analysis of tidal open boundaries

Tidal oscillations in the SCS are mainly co-oscillating tides forced by tidal wave motions on the Pacific Ocean and the Indian Ocean. The Pacific Ocean tides reach the SCS not only through the Luzon Strait but also through the Celebes Sea, while the Indian Ocean tides reach the SCS through the Andaman, Lombok and Flores Seas. A sensitivity analysis was conducted of the various tidal wave source boundaries including Andaman Sea, Flores Sea and Celebes Sea controlling tidal wave system in MDC.

Fig. 5a, b and c show the calculated differences of phases and amplitudes for the M_2 tide when excluding the Andaman, Flores and Celebes open boundaries. When excluding the Andaman and Flores boundaries, the change of the M_2 amplitude around the MDC is roughly 1–2 cm, increasing to 5–8 cm nearby Camau spit. Meanwhile, the boundary at Celebes strongly influences the eastern coastal Mekong regions with differences for the M_2 semidiurnal amplitude reaching as high as 15 cm. The differences of the co-phase lines are also limited in the case of excluding the Andaman and Flores boundaries. Meanwhile there are significant differences of the co-phase lines, roughly 30–40 min, in the south of the Mekong river mouth when excluding the Celebes boundary condition. The position of the amphidromic point shows a small change in the GoT, while the amphidromic point excluding the Flores boundary seems to be stationary. Comparison between the three open boundaries of Andaman, Flores and Celebes, the Celebes open boundary has the strongest effect on the semidiurnal tide in the coastal Mekong region, while the role of the Flores boundary is almost negligible.

Fig. 5d, e and f indicate the simulated changes of phases and amplitudes of the K_1 tide as a result of eliminating Andaman, Flores and Celebes open boundaries, respectively. Like for the M_2 semidiurnal tide, the incoming K_1 semidiurnal tidal wave from the Celebes Sea influences the MDC more strongly compared with the Andaman and Flores open boundaries. The differences of the K_1 diurnal amplitudes and co-phase lines for a closed Celebes boundary are definitely significant, reaching 25 cm and over 2 h, respectively. Meanwhile, the K_1 tidal wave propagation from the Andaman and Flores boundaries is smaller than that from the Celebes boundary to the coastal Mekong region with a difference of the K_1 diurnal amplitude of roughly 5–10 cm. While the tidal wave from the Flores Sea affects the change of co-phase lines of K_1 diurnal component with an average of about 35 min, the effect of Andaman Sea to K_1 tidal wave system in MDC is negligible. The results illustrate that the tidal incoming wave from the Celebes open boundary also plays an important role in the tidal wave system in the Mekong coastal region; hence it should not be neglected in simulating tidal wave propagation in the SCS in general and on the MDC in particular.

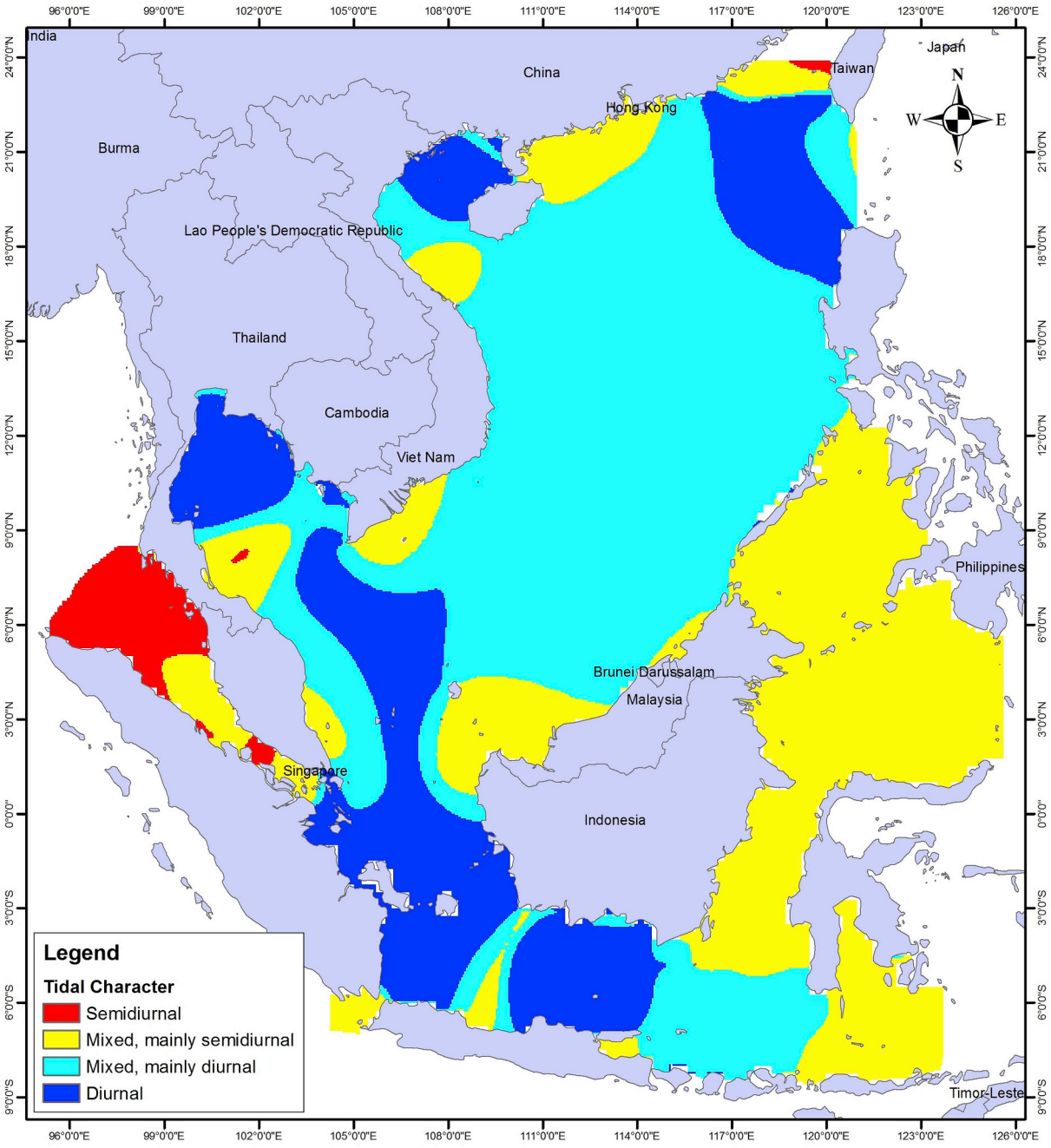

Fig. 4. Tidal character in the South China Sea.

4. Discussion

4.1. The shoaling and resonance effect

Although the shoaling and resonance processes are explained through the theoretical analysis of section 3.1.1, schematised numerical experiments were established to more firmly demonstrate these effects. The schematization concerns the use of three simplified topographies including a quasi-original case (Fig. 6a), the narrow Mekong deltaic shelf case (Fig. 6b) and the flat Mekong deltaic shelf case (Fig. 6c). Inspired by the results of the sensitivity analysis, the tidal wave system on the Sunda Shelf can be considered to be similar to the tidal wave propagation in a semi-enclosed basin because of the weak role of the Andaman and Flores open boundaries. The simplified models were forced at the open boundary of the SCS with an M_2 tidal amplitude and phase of 0.18m and 300° respectively. Fig. 6b and e shows that the wide scale of Mekong deltaic shelf significantly influences the resonance phenomenon. The M_2 amplitude decreases considerably along the MDC when the Mekong deltaic shelf is made narrower. Furthermore, Fig. 6c and f elucidate the importance of the topography for the effects of shoaling and tidal resonance when changing the slope as well as the length of schematised shelf. With a flat topography equal to that of the Mekong deltaic shelf, the M_2 amplitude along the MDC is no longer amplified.

4.2. Radial tidal currents

Based on the flood and ebb current fields as well as the tidal current ellipses (Fig. 3a, b, c, d), it is hypothesized that the interaction between the nearshore amplified amplitude and the offshore low amplitude due

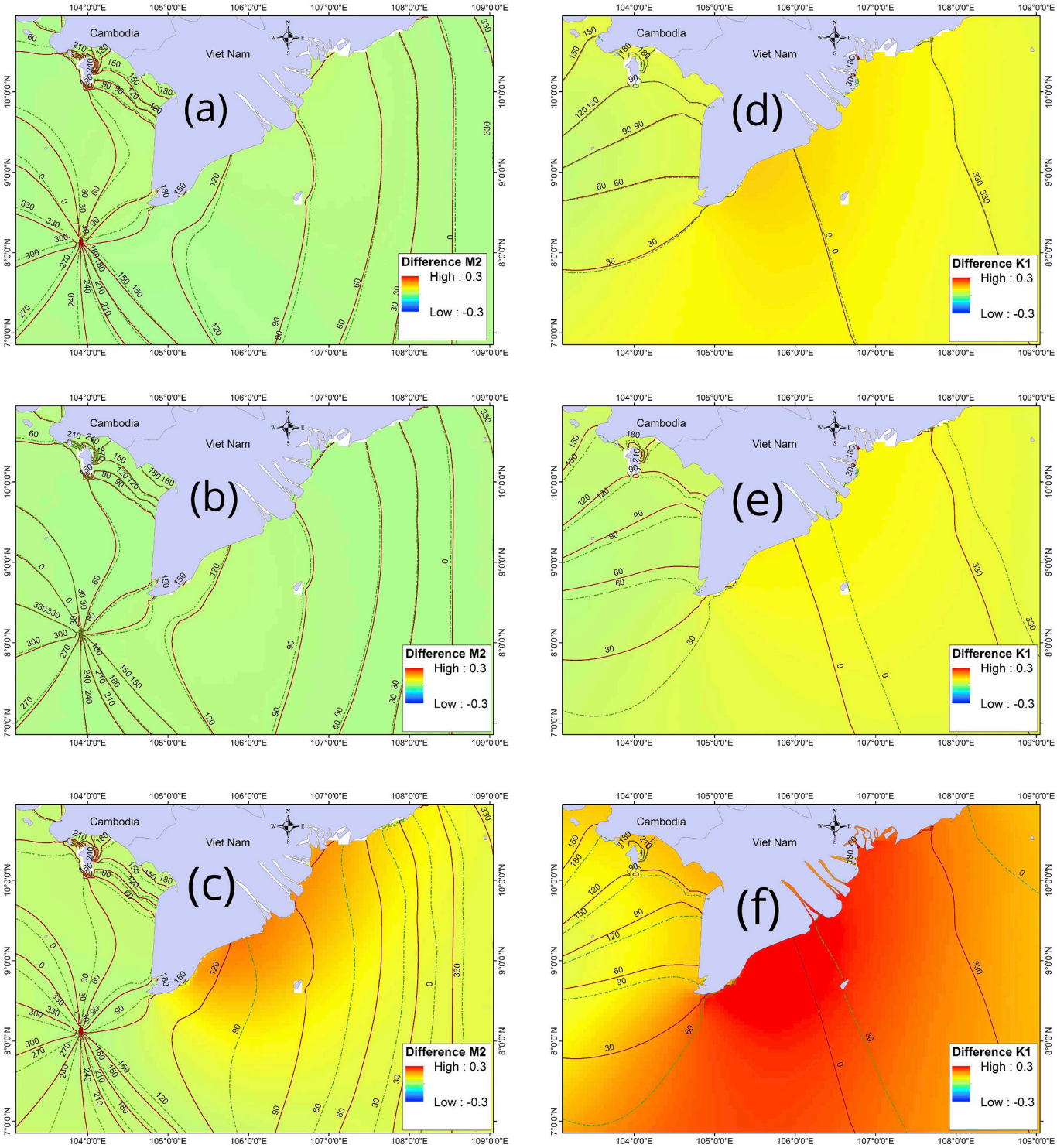

Fig. 5. Phase and amplitude difference of M_2, K_1 if ignoring Andaman (a,d), Flores (b, e), Celebes (c, f) boundaries, respectively, with brown solid and dashed green lines represent the co-phase lines of case original condition and case of excluding boundary. (For interpretation of the references to colour in this figure legend, the reader is referred to the Web version of this article.)

to the basin geometry and the shallow, sloping topography creates convex hydraulic gradients leading to radial tidal currents on the Mekong deltaic shelf. To deepen our insight in processes controlling the radial tidal current in the south of Mekong estuaries, schematised experiments were developed with different simplified geometry including the quasi-original case as section 4.1 (Fig. 6a), an extended GoT case (Fig. 7b) and an extended SCS case (Fig. 7c). The schematised models were forced at the open boundary at SCS with M_2 tidal amplitude and phase of 0.18m and 300° respectively as in the reality.

When the incident tidal wave from the SCS propagates to the Sunda Shelf and meets the reflected tidal wave from the western end of the Malaysian coast, this results in a standing wave in this semi enclosed area:

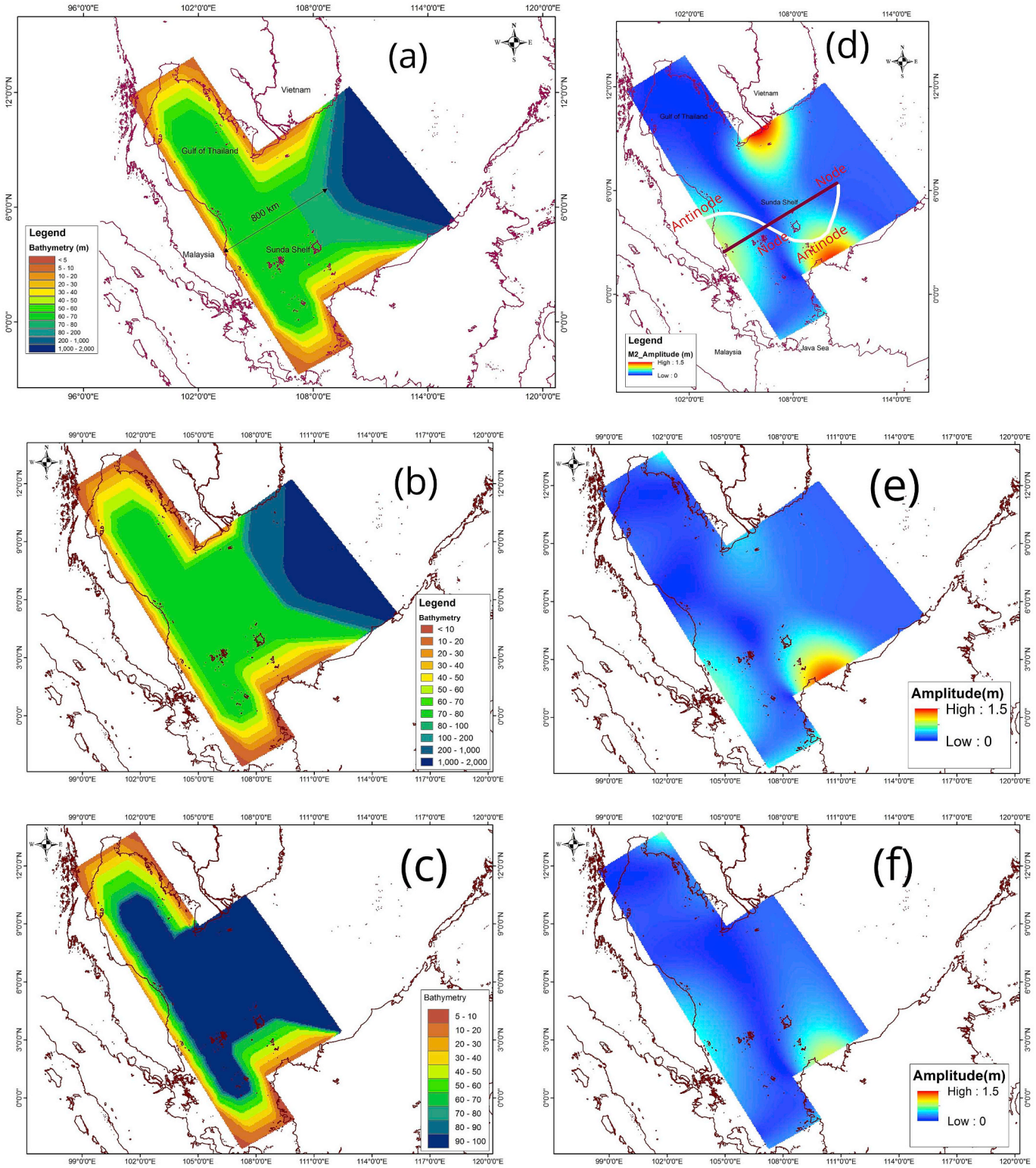

Fig. 6. Schematised experiments including topography and M_2 co-amplitude charts of the quasi-original case (a) and (d), the narrow shelf case (b) and (e) and the flat topography of Mekong deltaic shelf case (c) and (f), respectively.

$$\eta(x,t) = \frac{1}{2}\frac{a}{\cos kL_b}\left|\underbrace{\cos(\omega t - k(x-L_b))}_{\textit{incident wave}} + \underbrace{\cos(\omega t + k(x-L_b))}_{\textit{reflected wave}}\right|$$

$$= a\frac{\cos(k(L_b - x))}{\cos kL_b}\cos\omega t$$

Where η is surface elevation at location x in a certain moment t along basin length L_b; α, ω, k are tidal amplitude, angular frequency, wavenumber. The amplitude of the tidal elevation along the basin varies according to cos ($k(L_b-x)$). The amplification occurs for basins with a basin length equal to an uneven multiple of a quarter wavelength.

The basin length L_b from the Sunda Shelf edge to the Malaysian coast is roughly 800 km with a mean depth of 55m. The wavelength L of M_2 in this region equals 1040 km; hence the basin length L_b is nearly

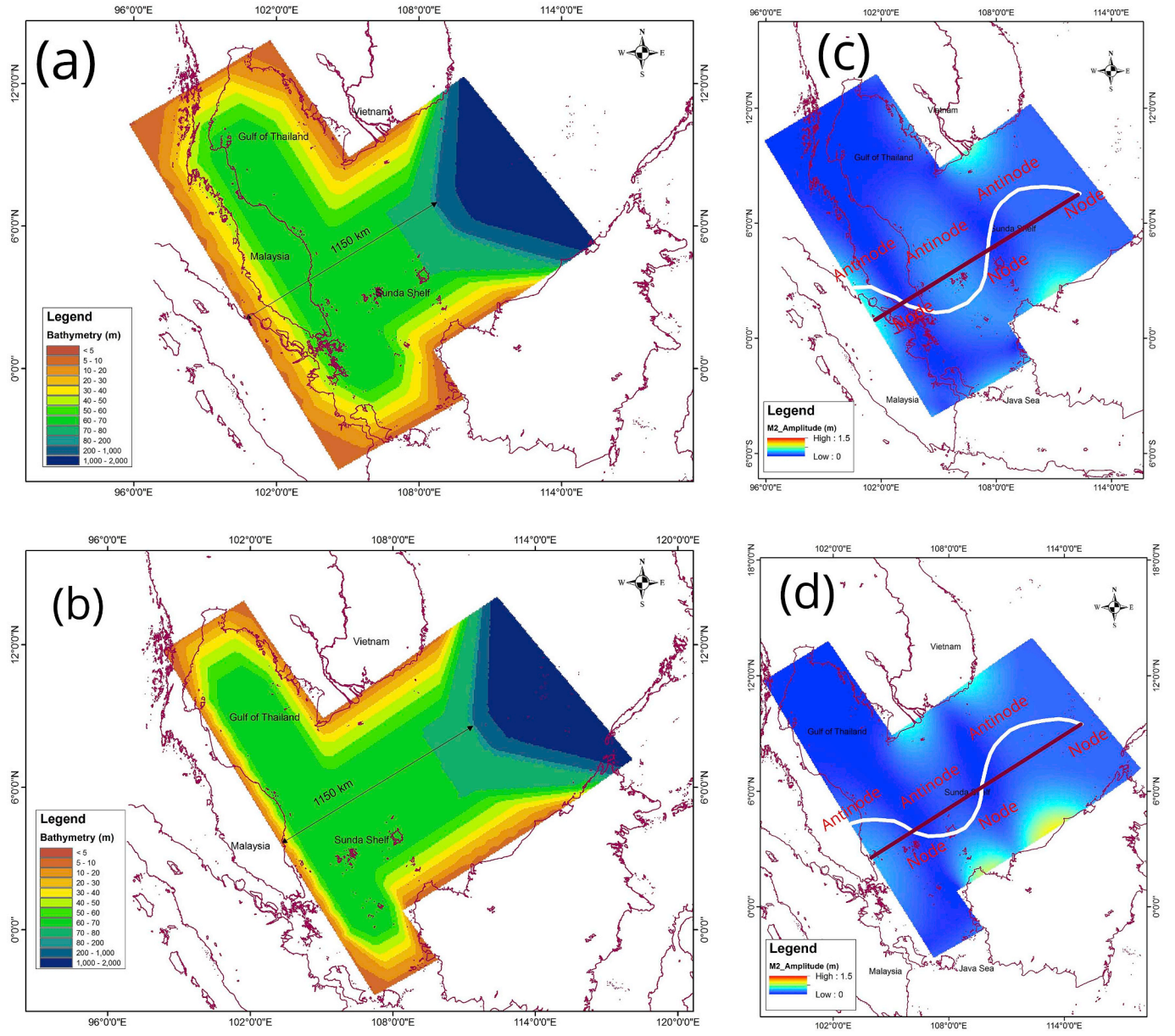

Fig. 7. Schematised experiments including topography and M_2 co-amplitude charts of extended Gulf of Thailand case (a) and (c) and extended South China Sea case (b) and (d).

three quarters wavelength M_2. Therefore, the Malaysian coast, the MDC and west Kalimantan are located at the antinodes of the standing tidal wave. In contrast, the area in between the MDC and the Malaysian coast is on a node of the standing tidal wave (Fig. 6d). Similarities in cases of extended GoT and SCS, standing tidal waves are produced and this leads to the nodes and antinodes systems in this basin (Fig. 7c and d). Specifically, the enlarged amplitude on the Mekong deltaic shelf is caused by shoaling and resonance effects due to the basin geometry, by the depth varying topography and by the position on the anti-nodal line of the standing wave.

Fig. 8a, b and c present the computational results of radial tidal currents in the schematised cases for the quasi-original geometry, the extended GoT and the extended SCS. Clearly, radial tidal currents occur in all three cases and there are only minor differences in locations as well as of magnitude for different basin geometries. Although the radial tidal currents compared to the quasi-original case are weaker, the radial tidal currents system are still present rather clearly in the extended SCS and GoT cases. Figs. 6d and 7c and d indicate that there are hydraulic gradients of convex form due to the large amplified amplitude nearshore and the low amplitude offshore. In conclusion, the responsible mechanisms for developing the radial tidal current system on the Mekong deltaic shelf are the convex hydraulic gradients of tidal amplitude due to the basin geometry and the depth varying topography.

4.3. Wind monsoon climate

While the tilting of the Earth produces climate seasonality, monsoon climate systems are a consequence of the land-sea temperature differences affected by solar radiation (Huffman et al., 1997). The monsoon climate is an atmospheric flow over Asia and is greatly variable depending on the Siberian High and the Arctic Oscillation (Wang et al., 2012). The Southeast Asian countries are controlled by the monsoon climate, which is charaterized by a large-scale seasonal reversal of the wind system (Serreze et al., 2010). The two main monsoon regimes are specifically named the northeast monsoon (winter monsoon) from November to April and the southwest monsoon (summer monsoon) from

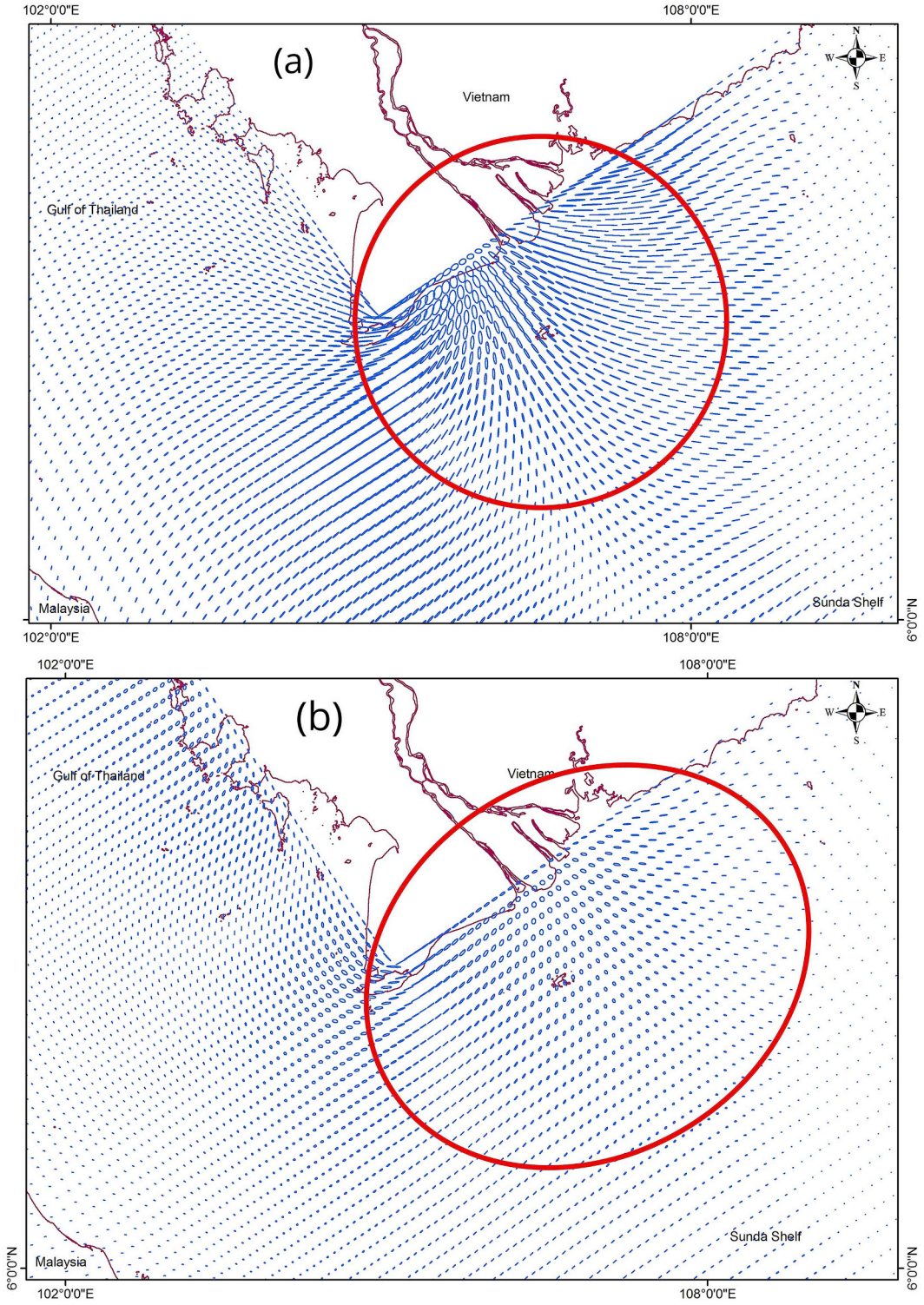

Fig. 8. Radial tidal currents for quasi-original case (a), extended Gulf of Thailand case (b) and extended South China Sea case (c).

late May to September. Furthermore, October is the transition month from the southwest to northeast monsoon seasons (Cruz et al., 2012). In this study, the wind monsoon climate data are collected from NOAA/NCEP in the period of 2011–2014 with the winter monsoon case from November to April and the summer monsoon case from May to October (See Fig. 9).

Fluctuations of sea level are superimposed upon regular tidal oscillations. In addition to the temporary and often dramatic variations in sea level due to tsunamis, hurricanes and other storms, variations in the predicted sea level frequently occur in association with the regular path of cyclonic disturbances across the coastal waters. These changes in sea level may be attributed in part to modifications to the changing atmospheric pressure and in part to the build-up or reduction of water at the coast due to the tangential stress of wind over the water surface. The pressure gradients in the horizontal momentum equations for water of constant density are computed by:

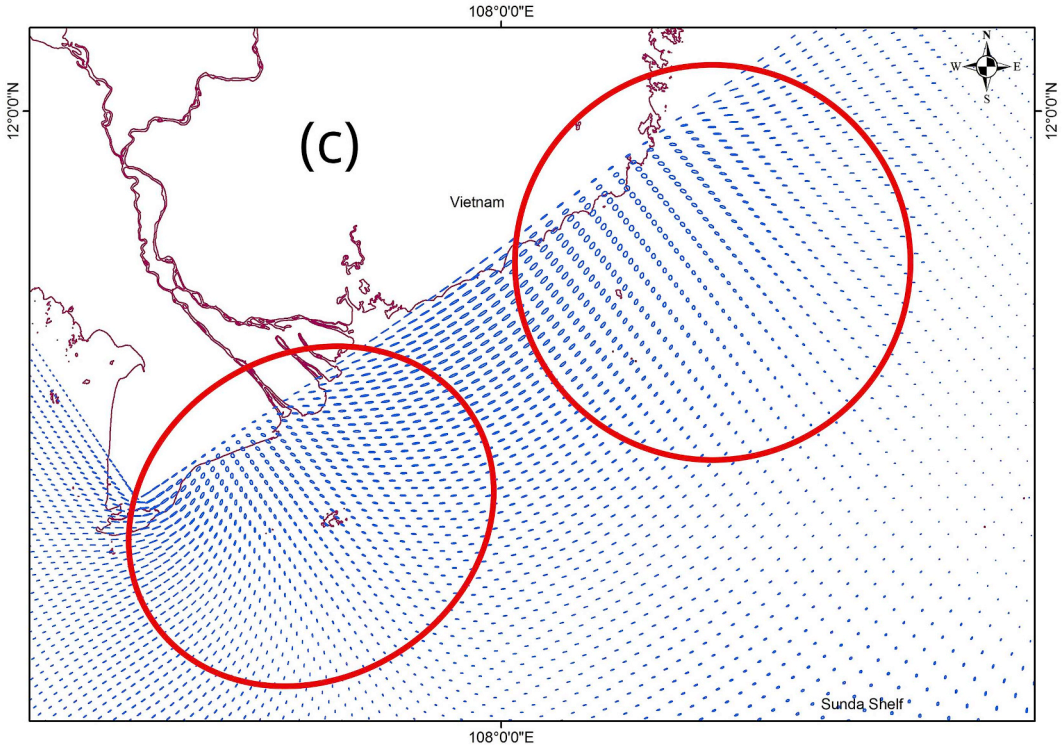

Fig. 8. (*continued*)

$$\frac{1}{\rho}P_x = g\frac{\partial\zeta}{\partial x} \qquad \frac{1}{\rho}P_y = g\frac{\partial\zeta}{\partial x}$$

Where ρ is the density of water, respectively, P_x and P_y are the horizontal pressure terms in the Cartesian horizontal x, y direction, ζ is water level above some horizontal plane of reference, g is acceleration due to gravity.

The steady state effect of wind stress on the free surface, wind is implemented as a uniform shear stress, based on the wind data available from NOAA included in the momentum equations. Wind stress magnitudes (Stuart, 1988) are computed from:

$$|\overrightarrow{\tau_w}| = \rho_\alpha C_d U_{10}^2$$

Where in ρ_α is the density of air (kg/m^3), U_{10} the wind speed 10 m above the free surface (m/s) and C_d the wind drag coefficient.

Besides, Ruessink et al. (2006) indicated that wind driven flow increased friction over the flood period of a tidal cycle more than it decreased friction over the ebb period, thus raising the friction over the tidal cycle and decreasing the tide current range. Changes in the bottom stress influencing tidal elevations and currents in a shallow sea during prevailing wind are shown by Jones and Davies (2008).

Fig. 10a and b shows the difference of M_2 semidiurnal tidal amplitudes and co-phase lines between original condition and wind climate monsoon condition. The results in the winter monsoon climate show that atmospheric forcing attenuates the M_2 tidal amplitude down to 2.5 cm at Soc Trang province on the eastern MDC, meanwhile the difference of the M_2 tidal phase is insignificant, viz. only 3–4 min. In the summer monsoon, the M_2 tidal amplitude is similarly damped until roughly 2 cm by wind forcing from a dominant southwest direction. The range of the M_2 tidal amplitude attenuation in the summer monsoon moves southward compared with the winter monsoon as a result of the seasonal difference of wind strength and atmospheric pressure due to the wind monsoon climate.

Similarly, the change of the K_1 semidiurnal tidal amplitudes and co-phase lines between the original condition and the wind climate monsoon condition are shown in Fig. 10c and d. Different from the M_2 semidiurnal tide, the K_1 diurnal tide is attenuated by an average of 1–2 cm in the western MDC due to the distribution of tidal characteristics around the MDC. The largest damped K_1 diurnal amplitude amounts to 2.5–2.6 cm along the Kiengiang coast in both the winter and summer monsoon climate. Like for the M_2 tide, the difference of K_1 tidal phases is minor, i.e. only 8–10 min. Therefore, the influence of the wind climate monsoon through the wind stress on the surface as well as the bed stress varies from region to region. The monsoon climate influences rather strongly on the semidiurnal tide in the eastern MDC, in contrast, the diurnal tide is affected quite considerably by the monsoon climate in the western region of Mekong delta.

4.4. Tide generating forces

Numerical models of tidal motion in coastal seas generally do not account for the direct local influence of the tide generating forces (TGF). The amount of water mass in these models is relatively small and the effect of these forces on the flow can be neglected. For coastal areas, the prescription of tidal forcing along open boundaries is sufficient in generating the appropriate tidal motion. In most numerical studies of tides in the Mekong coastal region, tidal open boundary forces (TOBFs) have been used to force tides and TGF has often been neglected. However, depending on the relative phases and magnitudes of the TOBF and TGF forcing, the interaction of different forcing components may lead to tides amplified or damped in continental shelf seas such as Bass Strait in Australia (Wijeratne et al., 2012), Gulf of Tartary in Japan (Odamaki, 1989), or Yellow Sea in China (Su et al., 2015). Because the water body in the semi-closed basin of SCS is even larger than in the above mentioned sea regions, the contribution of the gravitational forces on the water motion should be considered to generate an accurate tidal motion in the SCS and relevant to the MDC. The intervention between TGF and TOBF forcing enlarges and diminishes the tidal amplitude (Gouillon et al., 2010). The sea level of two tidal waves from TOBF and TGF of the same frequency can be expressed as:

$$\eta(t) = \eta_g(t) + \eta_o(t) = \alpha_g \cos(\omega t - \theta_g) + \alpha_o \cos(\omega t - \theta_o)$$

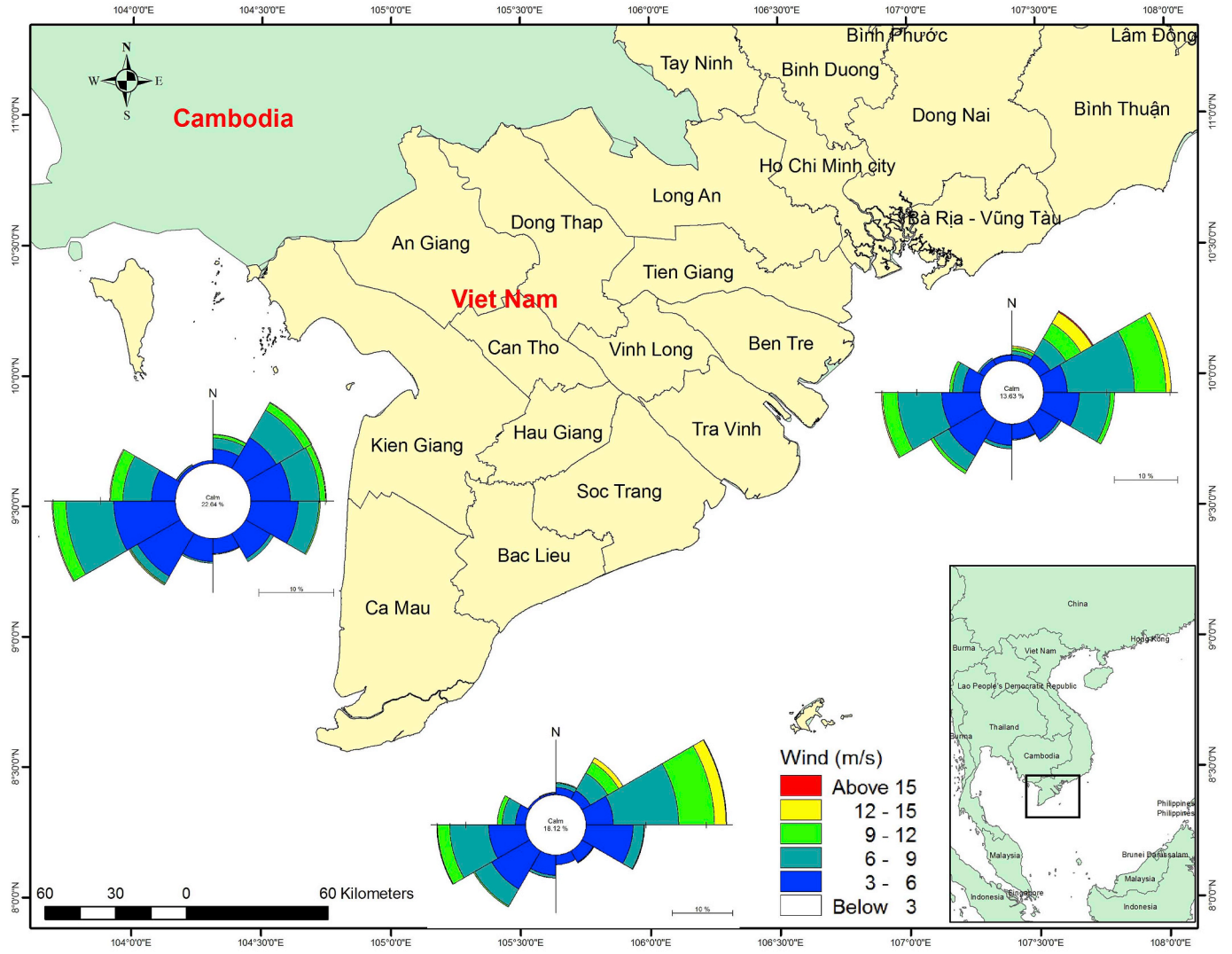

Fig. 9. Wind rose maps in Mekong deltaic coast.

Where η is the sea level at time t; g, o denotes the TGF case and TOBF case, respectively; α is the selected component's amplitude; ω is the selected tidal component's frequency; and θ is the selected tidal component's phase.

In the case denoted noTGF, the TGFs are ignored and the results are compared with the quasi-original condition case (OC) to examine the effect of TGF on the tidal motions. Fig. 11a and b shows the calculated differences of phase and amplitude of the M2 semidiurnal tide and K_1 diurnal tide between the cases OC and noTGF. Generally, the TGF influences the tidal wave system on the eastern MDC more than on the western MDC for both the M_2 and K_1 tidal components. For the M_2 tidal wave system, the change of the amplitude is relatively significant for the coastal eastern region of Mekong delta amounting approximately 5–8 cm, while the change of amplitude is only 1–1.6 cm in the western region. There is a relatively minor difference in the co-phase lines of the M_2 semidiurnal tide being roughly 10–15 min and in the position of the amphidromic point in the GoT that moves northwest over a distance of roughly 30 km. In the K_1 tidal wave system, changes of the amplitude on eastern and western MDC are on average 5 cm and 2 cm, respectively. The change of the co-phase lines of the K_1 diurnal tide is relatively significant compared to the M_2 tide with a co-phase difference of nearly 40–45 min. In conclusion, whether to include the TGF depends on the geographical region of interest.

5. Conclusions

A two-dimensional tidal model is constructed with high resolution to allow the simulation of accurate tidal wave propagation in the South China Sea (SCS, also known as the East Sea) as well as along the Mekong Deltaic Coast (MDC). According to the validation of the simulated tidal modelling, this model shows a good capability to reproduce the tidal wave system in the SCS and along the MDC. The mechanism of tidal wave propagation along the MDC is numerically investigated in detail for the M_2, S_2, K_1, O_1 tidal components that earlier studies have not considered.

The results indicate that the semidiurnal and diurnal tides propagate in the SCS mainly through the Luzon Strait. Meanwhile a small part of it moves to the Gulf of Tokin, mostly continuing to flow toward the southwest. After the tidal wave reaches the Sunda Shelf edge, a part of its turns into the GoT and another part spreads southwards to the Sunda Shelf end and Java Sea.

This study reveals that the tidal current ellipses of the M2 tide indicate strong currents occurring on the eastern coast of the Mekong delta, while weak currents occur on the western coast. Moreover, radial tidal currents are found to occur near the southern Mekong River mouths, which have never been documented before. A series of numerical, geometrically and topographically schematised experiments

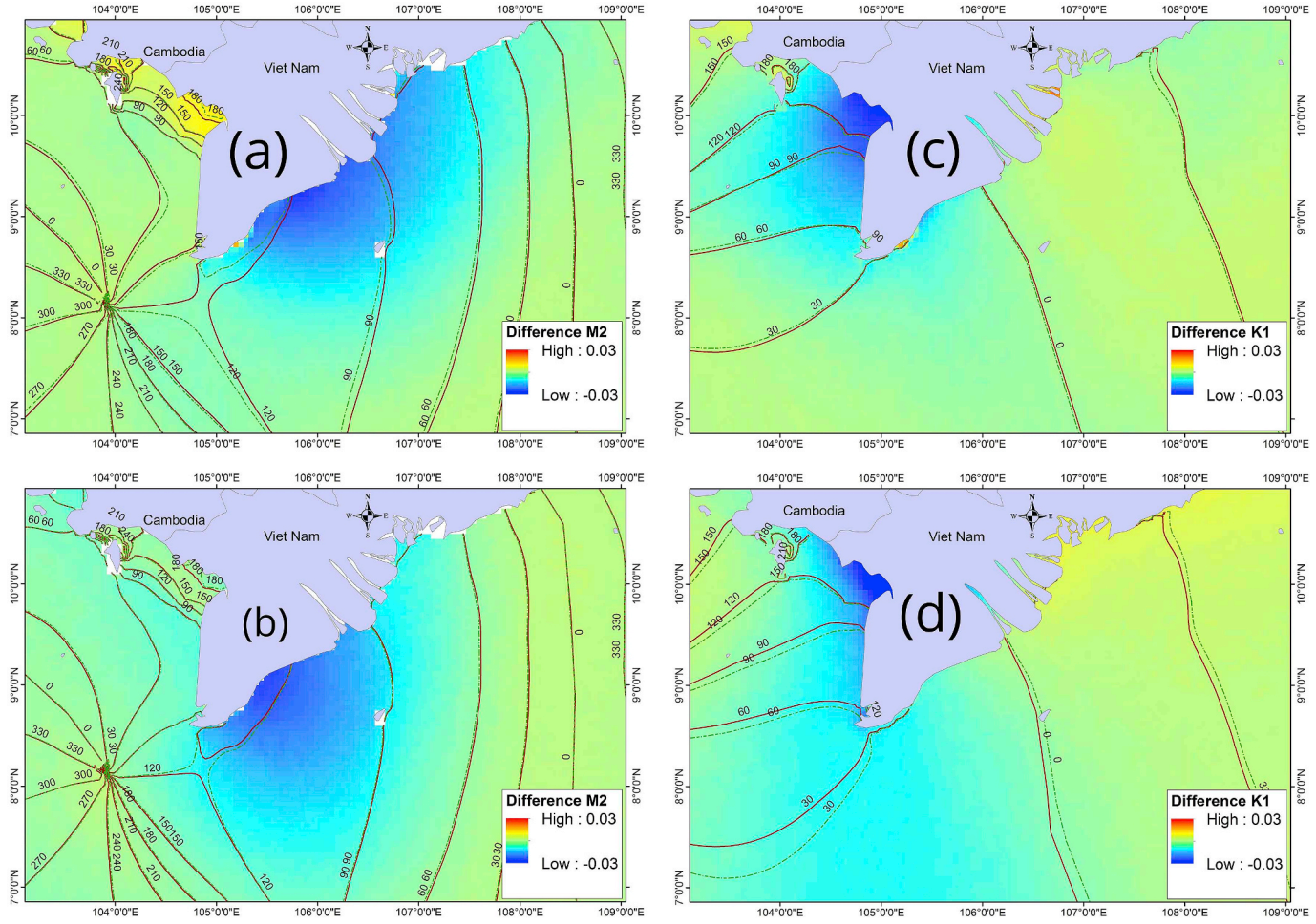

Fig. 10. Phase and amplitude difference of M_2, K_1 in case of wind climate monsoon in winter (a, c) summer (b, d), solid brown and dashed green lines represent the co-phase lines of case original condition and case of wind monsoon climate. (For interpretation of the references to colour in this figure legend, the reader is referred to the Web version of this article.)

were conducted to reveal the mechanisms responsible for establishing this radial tidal current system. Based on the result of these experiments, it is hypothesized that convex hydraulic gradients resulting from the spatial variation of the tidal amplitude due to basin geometry and depth varying topography leads to the formation of the radial tidal current system.

This study also shows that the tidal induced residual current increasing in the southeastward of the shallow coastal region of the Mekong delta is strongest along the Camau peninsula amounting to roughly 10–15 cm/s. This result will help understanding

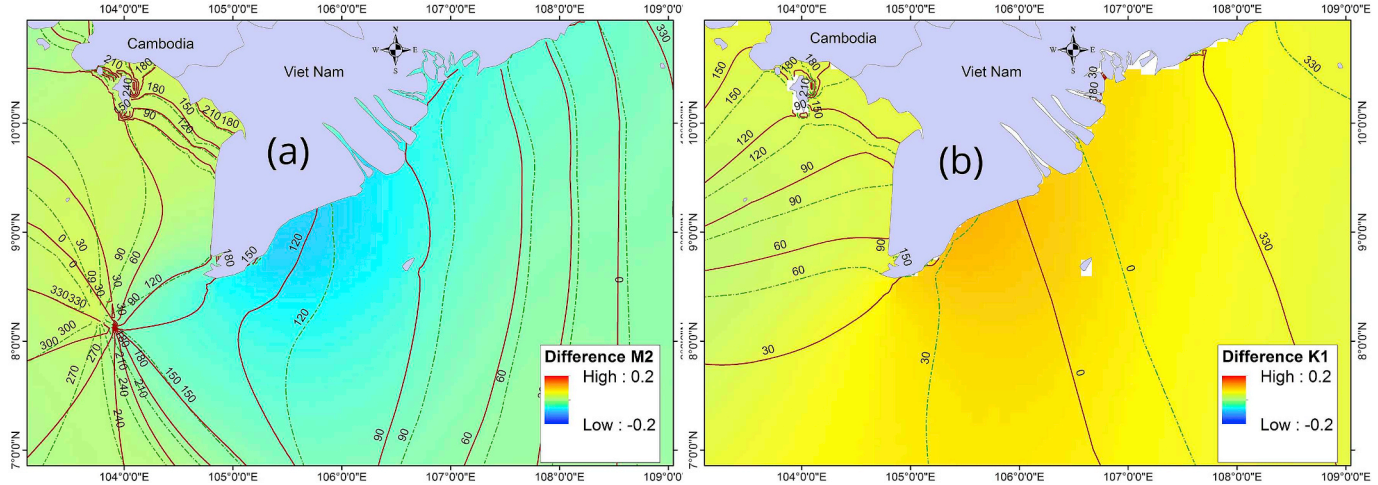

Fig. 11. Phase and amplitude differences of M_2 (a), K_1 (b) in case of excluding TGF; solid brown and dashed green lines represent the co-phase lines of case original condition and case noTGF. (For interpretation of the references to colour in this figure legend, the reader is referred to the Web version of this article.)

morphodynamic process along the MDC. Besides, an improved geographical distribution map of tidal characteristics in the whole SCS was developed by this study.

A sensitivity analysis illustrates that the tidal incident waves from the Andaman and Flores open boundaries influence the tidal wave system in the coastal Mekong region weakly, while the tidal incoming wave from the Celebes open boundary plays an important role. It is concluded that the tidal open boundary at Celebes should not be neglected in simulating the tidal wave propagation in SCS in general and the MDC in particular.

The natural oscillation periods of the Gulf of Tokin, the GoT and the SCS are found to be more or less of diurnal. Although both the SCS and the GoT are dominated by diurnal tides, semidiurnal tides dominate in the eastern MDC, which is enclosed by those seas. Most previous studies have not explained this remarkable characteristic. By means of Green's law, the formula of Clarke and Battisti (1981) and the theory of standing waves, this study demonstrates that the large amplified M_2 semidiurnal amplitude leads to a prevailing mixed semidiurnal tide caused by not only the shoaling effect and the oscillation resonance phenomenon on this continental shelf but also by its position on the anti-node line of the standing wave.

For the first time, the effect of the wind monsoon climate on the tidal wave system in this region is investigated. The results reveal that atmospheric forcing of the monsoon climate could cause damped or amplified tides along the MDC. The monsoon climate influences rather strongly on the M_2 semidiurnal tide system in the eastern MDC, meanwhile the monsoon climate controls the K_1 diurnal tide in the western region of Mekong delta.

Inclusion of the TGFs influencing the tidal wave system on MDC has not been considered before. Based on results of this study, it is suggested that the TGFs need to be considered for accurate model simulation depending on the geographical region of interest. Our findings contribute to understanding the processes of tidal wave propagation from the deep ocean into the SCS and to the shallow flats of the MDC. The present study employed a two-dimensional model with depth-averaged tidal dynamics; other effects such as baroclinic forcing is excluded in simulating tidal wave propagation. Hence, a 3D baroclinic model approach could be considered to achieve an even higher accuracy of tidal wave propagation along the MDC.

Acknowledgments

This research was funded by a scholarship of Vietnam government and TU Delft. We are grateful to the Institute of Coastal and Offshore Engineering and Southern Institute of Water Resources Research in Vietnam to support a part of measurement data for this study. The helpful comments of Gerrit Jen Schiereck are also appreciated.

Appendix A. Supplementary data

Supplementary data to this article can be found online at https://doi.org/10.1016/j.ecss.2019.01.026.

Appendix

Table A.1
Comparison of the harmonic constants between observed and calculated results for four primary constituents

No	Station name	LONG	LAT	S2						
				Observation		Calculation		dH	dG	VD
				Amp (cm)	Phase	Amp (cm)	Phase (deg.)	(cm)	(deg.)	(cm)
1	YU LIN KAN	109.606	18.19	6.8	335.2	10.9	326.6	−4.1	8.6	4.3
2	PAK HOI	109.145	21.529	10.6	353	14.7	344.1	−4.1	8.9	4.6
3	DO SON	106.808	20.667	4.3	136	9.9	139.9	−5.6	−3.9	5.6
4	HON NE	106.006	19.918	9.8	142	19.2	137.3	−9.4	4.7	9.5
5	HON NIEU	105.777	18.81	10	114	19.3	118.5	−9.3	−4.5	9.4
6	QUANG KHE	106.464	17.671	5.2	91	7.4	97.3	−2.2	−6.3	2.3
7	DA NANG	108.214	16.127	5.8	10	8.2	5.0	−2.4	5.0	2.4
8	QUI NHON	109.212	13.732	7	7	9.9	352.5	−2.9	14.5	3.6
9	CAM RANH	109.159	11.858	8.5	15	10.7	357.2	−2.2	17.8	3.7
10	PHU QUY	108.967	10.497	7.8	36.8	11.2	29.3	−3.4	7.5	3.7
11	KE GA	107.969	10.689	15.8	68	17.4	59.9	−1.6	8.1	2.8
12	VUNG TAU	107.086	10.305	30.7	111	38.5	120.2	−7.8	−9.2	9.5
13	CON DAO	106.593	8.656	28	142	29.1	143.0	−1.1	−1.0	1.2
14	MY THANH	106.193	9.432	37	141	41.1	146.7	−4.1	−5.7	5.7
15	GANH HAO	105.458	9.037	39	177	47.5	181.7	−8.5	−4.7	9.2
16	CA MAU	104.78	8.58	8	171	19.3	179.0	−11.3	−8.0	11.5
17	Tammassu	104.796	9.006	2.3	186	6.4	178.1	−4.1	7.9	4.1
18	HA TIEN	104.494	10.35	1.9	214	2.2	218.8	−0.3	−4.8	0.3
19	THO CHU	103.444	9.272	2	54	1.9	61.6	0.1	−7.6	0.3
20	KOMPONG SOAM	103.483	10.62	5.5	93	3.9	99.1	1.6	−6.1	1.7
21	SATTAHIP	100.859	12.622	12.2	225	5.0	231.0	7.2	−6.0	7.3
22	KOH HLAK	99.245	10.427	1.3	217	2.5	205.9	−1.2	11.1	1.3
23	PATTANI	101.325	6.943	4.5	350	8.2	1.2	−3.7	11.2	3.9
24	TELOK TEKEK	104.144	2.785	18.3	327	20.8	304.9	−2.5	22.1	7.9

(*continued on next page*)

Table A.1 (*continued*)

No	Station name	LONG	LAT	S2						
				Observation		Calculation		dH	dG	VD
				Amp (cm)	Phase	Amp (cm)	Phase (deg.)	(cm)	(deg.)	(cm)
25	TEBON ISLET	107.118	0.582	3	171.8	8.2	182.4	−5.2	−10.6	5.3
26	SELAT PENINTING	106.263	3.225	6	276	2.5	277.8	3.5	−1.8	3.5
27	POELOE LAOET	107.992	4.741	4	86	8.2	83.9	−4.2	2.1	4.2
28	PALOH	109.275	1.807	25	156.5	31.5	144.7	−6.5	11.8	8.7
29	TELOK PLAN	113.085	3.264	8	26	14.7	37.4	−6.7	−11.4	7.1
30	PALAU MANGALUM	115.592	6.198	10.4	358	12.7	349.6	−2.3	8.4	2.9
31	ULUGAU BAY	118.77	10.104	8	345	15.0	329.2	−7.0	15.8	7.6
32	SANTA CRUZ	119.948	15.739	1.7	323	6.1	331.6	−4.4	−8.6	4.5
33	NAGABUNGAN	120.56	18.498	5.8	214.9	2.6	201.2	3.2	13.7	3.4
34	KAO-HSIUNG	120.252	22.618	7.9	81.9	2.0	92.8	5.9	−10.9	6.0
35	CHAUAN BAY	117.292	23.609	28	80.4	39.3	84.2	−11.3	−3.8	11.5
36	HONGKONG	114.207	22.249	16.2	298.9	13.4	295.1	2.8	3.8	3.0
37	NAOZHOU DAO	110.589	20.927	34.9	23	40.4	31.3	−5.5	−8.3	7.7
38	NORTHDANGERREEF	114.31	11.469	10	347	15.2	341.3	−5.2	5.7	5.3
39	SCARBOROUGHSHOA	117.765	15.137	10	340	6.9	331.1	3.1	8.9	3.4
40	LES PARACELS	111.617	16.557	7.7	353	8.3	348.3	−0.6	4.7	0.9
41	PRATASREEF	116.716	20.678	6	267.1	2.7	284.6	3.3	−17.5	3.5
Average SVD										5.0
RMSE								5.2	9.5	
	Station name	LONG	LAT	K1						
				Observation		Calculation		dH	dG	VD
				Amp (cm)	Phase	Amp (cm)	Phase (deg.)	(cm)	(deg.)	(cm)
1	YU LIN KAN	109.606	18.19	28.5	310	23.4	316.1	5.1	−6.1	5.8
2	PAK HOI	109.145	21.529	86.2	102	79.6	105.2	6.6	−3.2	8.1
3	DO SON	106.808	20.667	67.5	106	59.8	112.5	7.7	−6.5	10.6
4	HON NE	106.006	19.918	54.4	107	49.8	113.7	4.6	−6.7	7.6
5	HON NIEU	105.777	18.81	43.6	113	36.8	122.4	6.8	−9.4	9.4
6	QUANG KHE	106.464	17.671	21.5	111	12.4	134.2	9.1	−23.2	11.2
7	DA NANG	108.214	16.127	19.5	305.7	21.3	304.6	−1.8	1.1	1.8
8	QUI NHON	109.212	13.732	32.9	316.2	22.9	312.3	10.0	3.9	10.2
9	CAM RANH	109.159	11.858	34.5	307.7	27.7	314.7	6.8	−7.0	7.8
10	PHU QUY	108.967	10.497	37	305.6	30.2	312.4	6.8	−6.8	7.9
11	KE GA	107.969	10.689	45.3	303	42.8	308.7	2.5	−5.7	5.0
12	VUNG TAU	107.086	10.305	59.5	327.7	55.2	331.9	4.3	−4.2	6.0
13	CON DAO	106.593	8.656	59	333.7	52.0	340.5	7.0	−6.8	9.6
14	MY THANH	106.193	9.432	64	342	58.2	345.1	5.8	−3.1	6.7
15	GANH HAO	105.458	9.037	67	3	70.1	11.4	−3.1	−8.4	10.5
16	CA MAU	104.78	8.58	33	23	41.0	31.7	−8.0	−8.7	9.7
17	Tammassu	104.796	9.006	18	107	25.8	116.0	−7.8	−9.0	8.5
18	HA TIEN	104.494	10.35	26.2	126.7	29.7	135.3	−3.5	−8.6	5.4
19	THO CHU	103.444	9.272	17	89	13.4	91.4	3.6	−2.4	3.6
20	KOMPONG SOAM	103.483	10.62	24.5	141.7	25.6	147.4	−1.1	−5.7	2.7
21	SATTAHIP	100.859	12.622	54.4	185.7	60.4	192.2	−6.0	−6.5	8.9
22	KOH HLAK	99.245	10.427	40.2	186.7	43.8	197.2	−3.6	−10.5	8.5
23	PATTANI	101.325	6.943	12.2	333.7	10.7	339.1	1.5	−5.4	1.9
24	TELOK TEKEK	104.144	2.785	43	25.2	48.6	36.4	−5.6	−11.2	10.6
25	TEBON ISLET	107.118	0.582	28	129.9	21.6	119.7	6.4	10.2	7.7
26	SELAT PENINTING	106.263	3.225	39	13.7	39.5	27.9	−0.5	−14.2	9.7
27	POELOE LAOET	107.992	4.741	36	349	37.0	353.0	−1.0	−4.0	2.8
28	PALOH	109.275	1.807	27	357.7	20.6	12.0	6.4	−14.3	8.7
29	TELOK PLAN	113.085	3.264	42	320.6	36.9	328.0	5.1	−7.4	7.2
30	PALAU MANGALUM	115.592	6.198	34.1	312.6	30.0	320.6	4.1	−8.0	6.1
31	ULUGAU BAY	118.77	10.104	31	312.7	25.8	301.7	5.2	11.0	7.5
32	SANTA CRUZ	119.948	15.739	25.7	313.7	20.3	321.2	5.4	−7.5	6.2
33	NAGABUNGAN	120.56	18.498	16.5	313.5	11.3	318.7	5.2	−5.2	5.4
34	KAO-HSIUNG	120.252	22.618	16.5	285	19.4	298.5	−2.9	−13.5	5.1
35	CHAUAN BAY	117.292	23.609	32	292.3	27.8	275.4	4.2	16.9	9.7
36	HONGKONG	114.207	22.249	36	299.8	29.1	316.0	6.9	−16.2	11.4
37	NAOZHOU DAO	110.589	20.927	44	314.7	36.5	332.4	7.5	−17.7	14.4
38	NORTHDANGERREEF	114.31	11.469	20	305.7	26.3	311.3	−6.3	−5.6	6.6

(*continued on next page*)

Table A.1 (*continued*)

	Station name	LONG	LAT	K1						
				Observation		Calculation		dH	dG	VD
				Amp (cm)	Phase	Amp (cm)	Phase (deg.)	(cm)	(deg.)	(cm)
39	SCARBOROUGHSHOA	117.765	15.137	30	330.7	25.4	327.8	4.6	2.9	4.8
40	LES PARACELS	111.617	16.557	26.8	306	22.9	310.7	3.9	−4.7	4.4
41	PRATASREEF	116.716	20.678	27.5	314.9	18.4	312.7	9.1	2.2	9.2
Average SVD										7.4
RMSE								5.7	9.3	
No	Station name	LONG	LAT	O1						
				Observation		Calculation		dH	dG	VD
				Amp (cm)	Phase (deg.)	Amp (cm)	Phase (deg.)	(cm)	(deg.)	(cm)
1	YU LIN KAN	109.606	18.19	28.7	271.0	27.1	287.8	1.6	−16.8	8.3
2	PAK HOI	109.145	21.529	94.7	51.0	98.9	64.0	−4.2	−13.0	22.3
3	DO SON	106.808	20.667	74.1	48.0	81.4	61.3	−7.3	−13.3	19.4
4	HON NE	106.006	19.918	69.1	50.0	63.1	62.0	6.0	−12.0	15.1
5	HON NIEU	105.777	18.81	58.9	54.5	51.0	69.0	7.9	−14.5	15.9
6	QUANG KHE	106.464	17.671	26.9	58.0	34.4	73.3	−7.5	−15.3	11.0
7	DA NANG	108.214	16.127	12.9	257.4	16.2	251.3	−3.3	6.1	3.6
8	QUI NHON	109.212	13.732	28.5	267.3	27.3	269.6	1.2	−2.3	1.6
9	CAM RANH	109.159	11.858	29.2	267.4	34.4	269.2	−5.2	−1.8	5.3
10	PHU QUY	108.967	10.497	31.3	263.3	30.4	270.4	0.9	−7.1	3.9
11	KE GA	107.969	10.689	37.7	265.0	37.0	272.8	0.7	−7.8	5.1
12	VUNG TAU	107.086	10.305	45.2	276.4	45.1	281.3	0.1	−4.9	3.9
13	CON DAO	106.593	8.656	45.0	290.4	44.0	296.8	1.0	−6.4	5.1
14	MY THANH	106.193	9.432	45.1	293.0	52.4	301.8	−7.3	−8.8	10.4
15	GANH HAO	105.458	9.037	44.7	310.0	51.4	315.8	−6.7	−5.8	8.2
16	CA MAU	104.78	8.58	19.0	325.0	25.1	311.3	−6.1	13.7	8.0
17	Tammassu	104.796	9.006	11.0	66.0	15.5	67.8	−4.5	−1.8	4.6
18	HA TIEN	104.494	10.35	12.8	88.0	17.6	85.0	−4.8	3.0	4.8
19	THO CHU	103.444	9.272	7.0	55.0	15.6	62.8	−8.6	−7.8	8.7
20	KOMPONG SOAM	103.483	10.62	18.4	98.4	23.1	100.1	−4.7	−1.7	4.8
21	SATTAHIP	100.859	12.622	42.0	125.4	48.5	132.9	−6.5	−7.5	8.8
22	KOH HLAK	99.245	10.427	26.8	134.4	31.5	142.0	−4.7	−7.6	6.1
23	PATTANI	101.325	6.943	7.3	279.4	5.7	287.8	1.6	−8.4	1.8
24	TELOK TEKEK	104.144	2.785	32.2	342.4	35.6	352.4	−3.4	−10.0	6.8
25	TEBON ISLET	107.118	0.582	27.0	43.9	28.2	53.6	−1.2	−9.7	4.8
26	SELAT PENINTING	106.263	3.225	29.0	327.4	32.5	342.0	−3.5	−14.6	8.5
27	POELOE LAOET	107.992	4.741	29.7	282.0	34.9	301.2	−5.2	−19.2	12.0
28	PALOH	109.275	1.807	14.0	294.7	21.1	294.0	−7.1	0.7	7.1
29	TELOK PLAN	113.085	3.264	36.0	268.4	35.0	277.6	1.0	−9.2	5.8
30	PALAU MANGALUM	115.592	6.198	31.1	274.4	29.2	272.4	1.9	2.0	2.2
31	ULUGAU BAY	118.77	10.104	28.0	266.4	22.9	246.0	5.1	20.4	10.3
32	SANTA CRUZ	119.948	15.739	21.9	258.4	22.9	273.6	−1.0	−15.2	6.0
33	NAGABUNGAN	120.56	18.498	17.4	268.4	17.4	270.5	0.0	−2.1	0.6
34	KAO-HSIUNG	120.252	22.618	15.9	259.7	19.5	251.2	−3.6	8.5	4.5
35	CHAUAN BAY	117.292	23.609	26.3	247.0	16.5	265.1	9.8	−18.1	11.8
36	HONGKONG	114.207	22.249	28.9	248.7	28.6	255.5	0.3	−6.8	3.4
37	NAOZHOU DAO	110.589	20.927	39.5	275.4	35.7	281.1	3.8	−5.7	5.3
38	NORTHDANGERREEF	114.31	11.469	30.0	256.4	26.7	271.3	3.3	−14.9	8.0
39	SCARBOROUGHSHOA	117.765	15.137	30.0	279.4	23.9	278.3	6.1	1.1	6.1
40	LES PARACELS	111.617	16.557	23.4	260.5	25.3	270.3	−1.9	−9.8	4.6
41	PRATASREEF	116.716	20.678	16.8	250.1	26.3	260.7	−9.5	−10.6	10.3
Average SVD										7.1
RMSE								4.9	10.4	

Table A.2
Measurement and simulation results of tidal current ellipses for four primary constituents

Location	Tidal constituents			
	M2	S2	K1	O1
Tien Giang	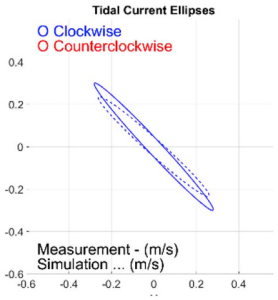	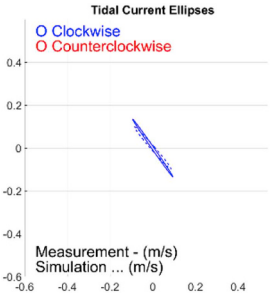	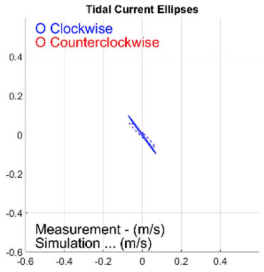	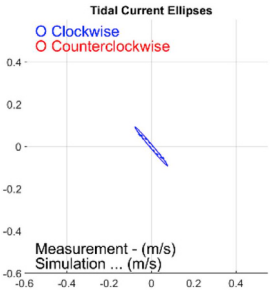
Tra Vinh	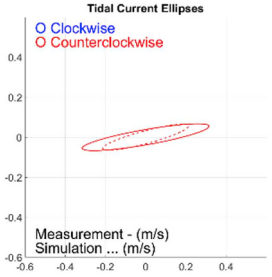	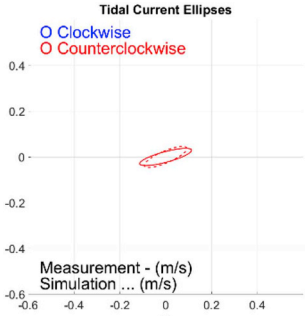	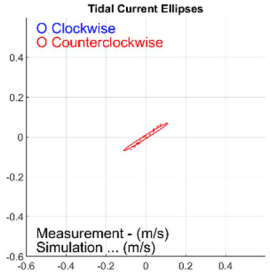	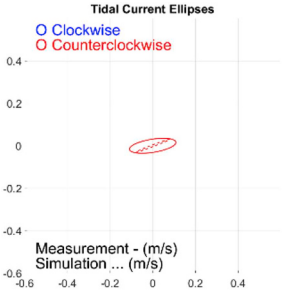
Ca Mau Spit	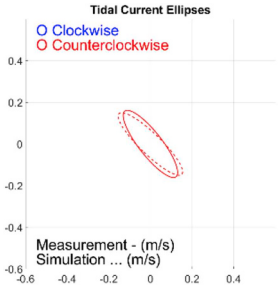	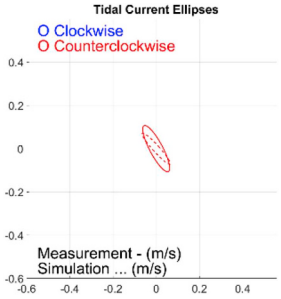	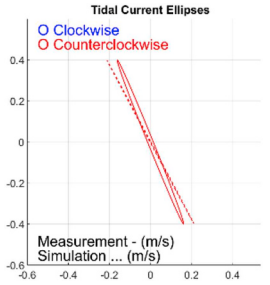	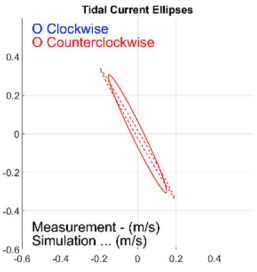
Western Ca Mau	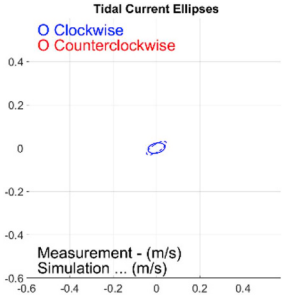	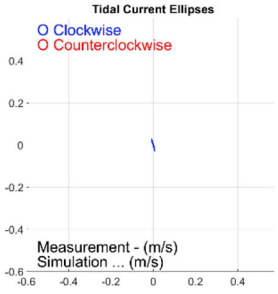	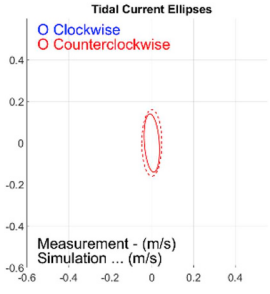	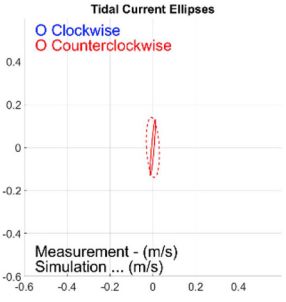

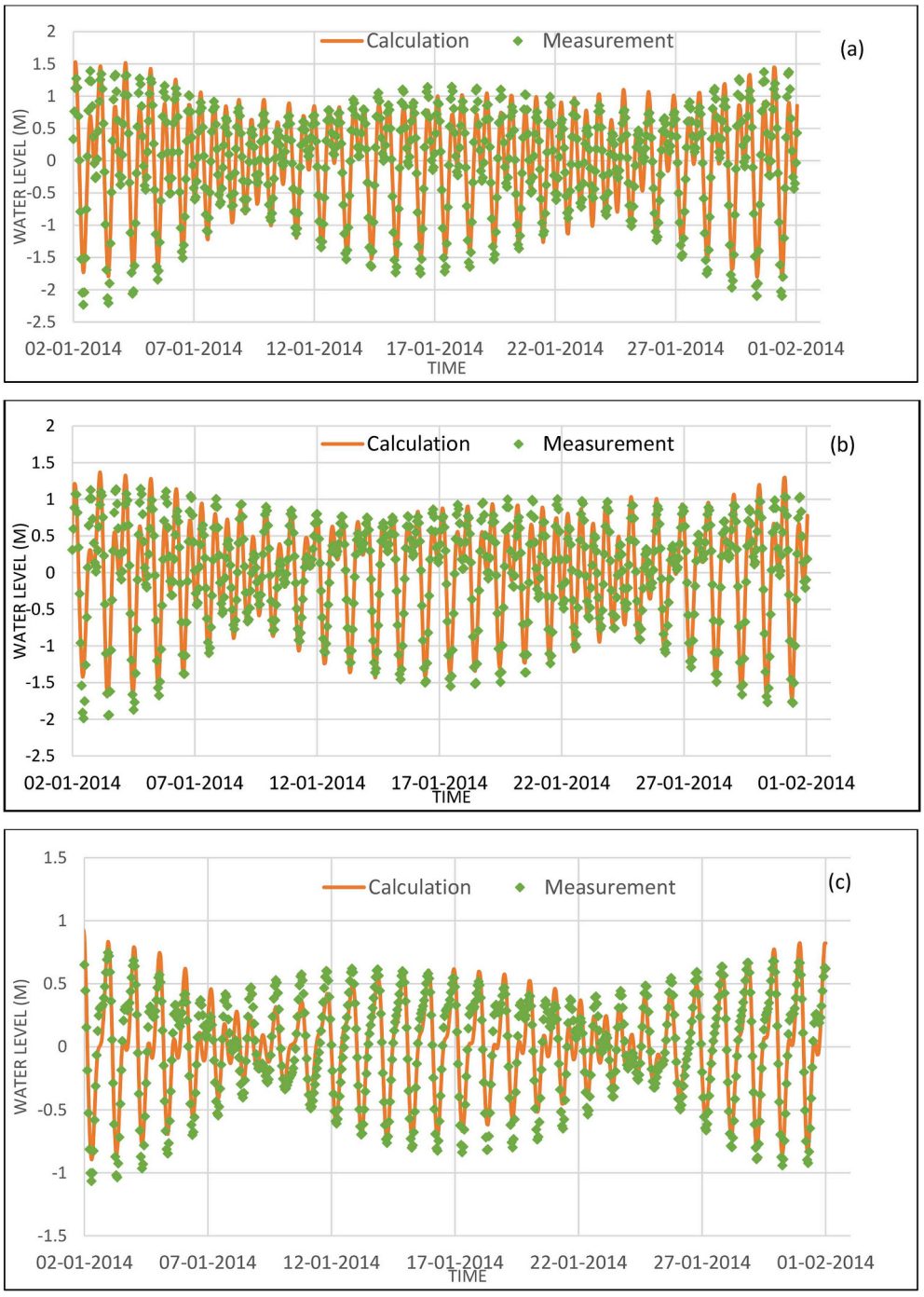

Fig. A1. Calculated and measured water level at Vungtau (a), Condao (b), Phuquy (c) stations.

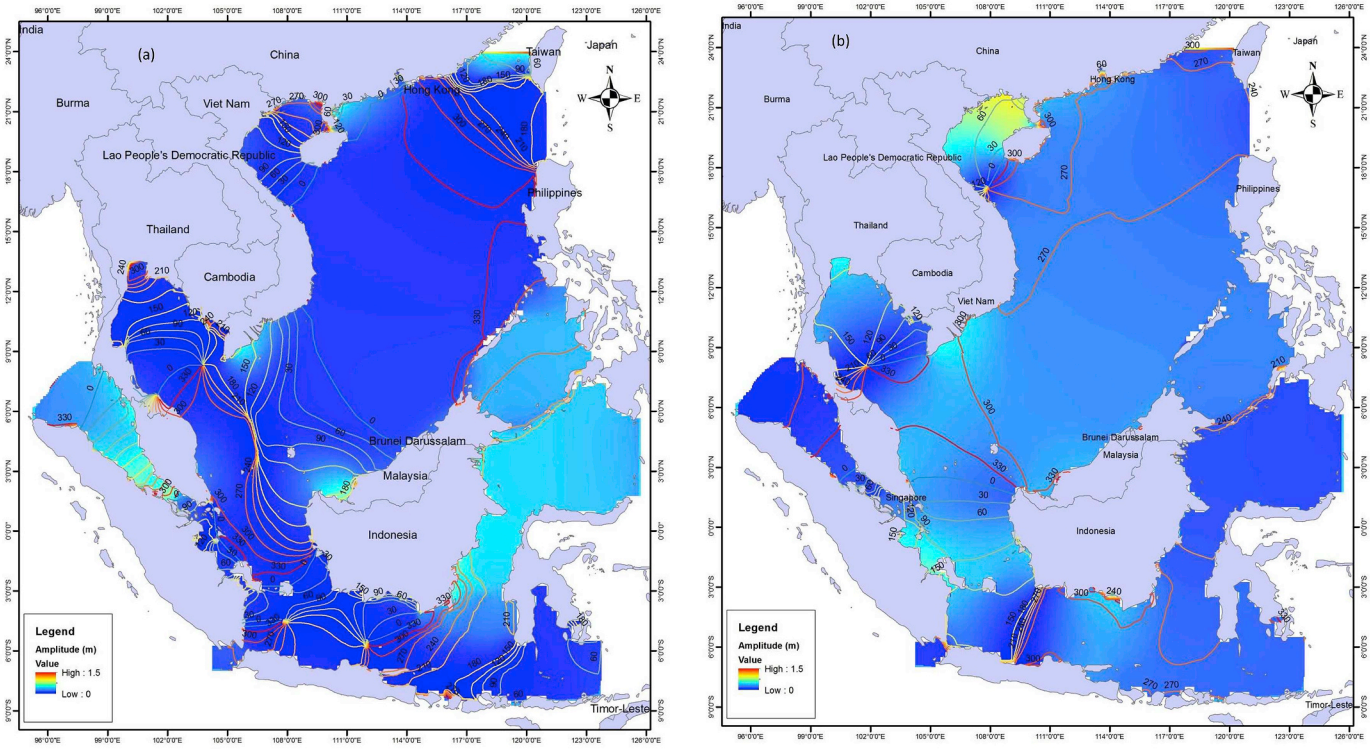

Fig. A2. Co-tidal chart of S2 (a), O1 (b).

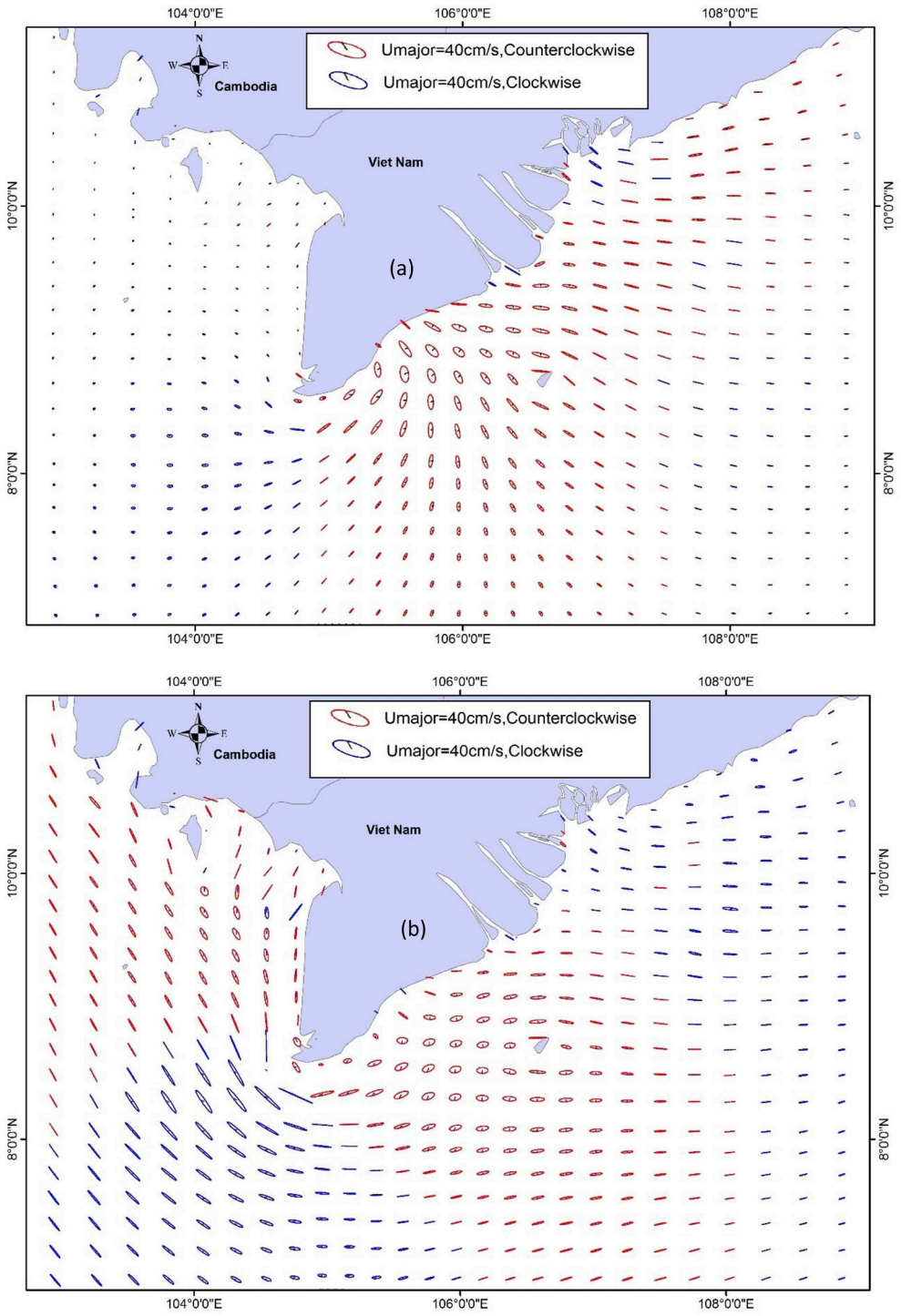

Fig. A3. Tidal current ellipses S2 (a) and O1 (b).

References

Clarke, A.J., Battisti, D.S., 1981. The effect of continental shelves on tides. Deep Sea Res. 28A, 665–682.

Cruz, F.T., Narisma, T.G., Villafuerte, M.Q., Cheng, K.U.C., Olaguera, L.M., 2012. A climatological analysis of the southwest monsoon rainfall in the Philippines. Atmos. Res. 122 (2012), 609–616.

Davis Jr., R.A., Hayes, M.O., 1984. What is a wave-dominated coast. Mar. Geol. 60, 313–329.

Defant, A., 1961. Physical Oceanography, vol. II. Pergamon Press, Oxford, pp. 598.

Delta Alliance, 2011. Mekong Delta Water Resources Assessment Studies – Vietnam-Netherlands Mekong Delta Masterplan Project. http://wptest.partnersvoorwater.nl/wp-content/uploads/2011/08/WATERRESOURCESfinaldraft.pdf, Accessed date: 17 April 2013.

Deltares, 2014. User manual, Delft3D Flow. Deltares, Delft, the Netherlands.

Fang, G., Kwok, Y.K., Yu, K., Zhu, Y., 1999. Numerical simulation of principal tidal constituents in the South China Sea, Gulf of Tokin and Gulf of Thailand. Cont. Shelf Res. 19, 845–869.

Gagliano, S.M., McIntire, W.G., 1968. Reports on the Mekong Delta, vol. 57. Coastal Studies Institute, Louisiana State University Technical Report, pp. 144.

Galloway, W.E., Hobday, D.K., 1983. Delta systems. In: Terrigenous Clastic Depositional Systems. Springer, New York, NY.

Gao, X., Wei, Z., Lv, X., Wang, Y., Fang, G., 2015. Numerical study of tidal dynamics in the South China Sea with adjoint method. Ocean Model. 92, 101–114.

Gerritsen, H., Schrama, E.J.O., Van der Boogaard, H.F.P., 2003. Tidal model validation of the seas of South East Asia using altimeter data and adjoint modelling. Proc. 30th IAHR Congress, Thessaloniki, 2003, vol. D. pp. 239–246.

Gouillon, F., Morey, S.L., Dukhovskoy, D.S., O'Brien, J.J., 2010. Forced tidal response in the Gulf of Mexico. J. Geophys. Res. Oceans 115 (C10050).
Hein, H., Hein, B., Pohlmann, T., 2013. Recent sediment dynamics in the region of Mekong water influence. Glob. Planet. Chang. 110, 183–194.
Hordoir, R., Polcher, J., Brun-Cottan, J.-C., Madec, G., 2006. Towards a parametrization of river discharges into ocean general circulation models: a closure through energy conservation. Clim. Dynam. 31 (7–8), 891–908.
Huffman, G.J., Adler, R.F., Arkin, P., Chang, A., Ferraro, R., Gruber, A., Janowiak, J., McNab, A., Rudolf, B., Schneider, U., 1997. The global precipitation climatology project (GPCP) combined precipitation data set. Bull. Am. Meteorol. Soc. 78, 5–20.
Institute of Coastal and Offshore Enginerring (ICOE), 2011. Vietnam government project of study on sedimentation and erosion in the along Camau spit, Vietnam. http://icoe.org.vn/index.aspx?aac=CLICK&aid=ARTICLE_DETAIL&ari=3097&lang=1&menu=de-tai–du-an-cac-nam&mid=178&parentmid=1002&pid=1&storeid=0&title=nhiem-vu-khcn-nam-2011 (inVietnamese).
Institute of Coastal and Offshore Enginerring (ICOE), 2014. Province project of morphodynamics in coastal zone of Travinh province, Vietnam. http://icoe.org.vn/index.aspx?aac=CLICK&aid=ARTICLE_DETAIL&ari=3100&lang=1&menu=de-tai–du-an-cac-nam&mid=178&parentmid=1002&pid=1&storeid=0&title=nhiem-vu-khcn-nam-2014 (in Vietnamese).
Institute of Strategy and Policy on natural resources and environment (ISPONRE), 2009. Vietnam Assessment Report on Climate Change, vol. 127.
IOC, IHO and BODC, 2003. 2003 in the body of the text that IOC, IHO and BODC. Centenary Edition of the GEBCO Digital Atlas. In: The Intergovernmental Oceanographic Commission and the International Hydrographic Organization as part of the General Bathymetric Chart of the Oceans. British Oceanographic Data Centre, Liverpool, U.K..
Jones, J.E., Davies, A.M., 2008. On the modification of tides in shallow water regions by wind effects. J. Geophys. Res. Oceans 113 (C05014). https://doi.org/10.1029/2007JC004310.
Lee, S., Lie, H.J., Cho, C.H., Kang, S.K., Teague, W.J., Chang, K., Song, K.M., Oh, K.H., 2011. Vertical structure of the M2 tidal current in the Yellow Sea. Ocean Sci. J. 46 (2), 73–84.
Lesser, G.R., Roelvink, J.A., van Kester, J.A.T.M., Stelling, G.S., 2004. Development and validation of a three-dimensional morphological model. Coast. Eng. J. 51, 883–915.
Nguyen, K.D., Guillou, N., Pham, N.N., 1998. A 3-D numerical study of the tidal circulation in the Mekong Delta Coastal Zones, Vietnam. In: International Workshop on the Mekong Delta, 23-27 February 1998, Chiang Rai, Thailand, pp. 57–71.
Nguyen, L.V., Ta, T.K.O., Tateishi, M., 2000. Late Holocene depositional environments and coastal evolution of the Mekong river delta, Southern Vietnam. J. Asian Earth Sci. 18 (4), 427–439.
Odamaki, M., 1989. Co-oscillating and independent tides of the Japan Sea. J. Oceanogr. Soc. Jpn. 45 (3), 217–232.
Proudman, J., 1953. Dynamical Oceanography. MethuenandCo. Ltd., London, pp. 409pp.
Ruessink, B.G., Houwman, K.T., Grasmeijer, B.T., 2006. Modeling the nonlinear effect of wind on rectilinear tidal flow. J. Geophys. Res. Oceans 111 (C10002). https://doi.org/10.1029/2006JC003570.
Saito, Y., Nguyen, V.L., Ta, T.K.O., Tamura, T., Kanai, Y., Nakashima, R., 2015. Tide and river influences on distributary channels of the Mekong River delta, vol. 2015 American Geophysical Union, Fall Meeting abstract #GC41F-1148.
Serreze, R.G., Barry, R.G., Chorley, R.J., 2010. Atmosphere, Weather and Climate. Routledge, Oxon.
Southern Institute of Water Resources Research (SIWRR), 2010. Project for measurements of bathymetry, hydrodynamics in estuaries and coastal zone of Mekong delta from 2009 to 2010. (in Vietnamese). http://www.siwrr.org.vn/?id=nckh5.
Southern Instiute of Water Resources Research (SIWRR), 2016. Lower Mekong Delta Coastal Zone. http://lmdcz.siwrr.org.vn/?lang=e.
Stelling, G.S., Kester, J.A.T.M.V., 1994. On the approximation of horizontal gradients in sigma co-ordinates for bathymetry with steep bottom slopes. Int. J. Numer. Methods Fluid. 18, 915–955.
Stuart, D.M., 1988. Coefficients for sea surface wind stress, heat flux, and wind profiles as a function of wind speed and temperature. J. Geophys. Res. 93 (C12), 15467. https://doi.org/10.1029/JC093iC12p15467.
Su, M., Yao, P., Wang, Z.B., Zhang, C.K., Stive, M.J.F., 2015. Tidal Wave Propagation in the Yellow Sea. Coast Eng. J. 57 (3), 1550008.
Ta, T.K.O., Nguyen, V.L., Tateishi, M., Kobayashi, I., Tanabe, S., Saito, Y., 2002. Holocene delta evolution and sediment discharge of the Mekong River, southern Vietnam. Quat. Sci. Rev. 21 (16–17), 1807–1819.
Tas, S., 2016. Coastal protection in the Mekong delta. Master thesis. . https://repository.tudelft.nl.
Unverricht, D., Szczucinski, W., Stattegger, K., Jagodzinski, R., Le, X.T., Kwong, L.L.W., 2013. Modern sedimentation and morphology of the subaqueous Mekong Delta, Southern Vietnam. Glob. Planet. Chang. 110, 223–235.
Unverricht, D., Nguyen, T.C., Heinrich, C., Szczucinski, W., Lahajnar, N., Stattegger, K., 2014. Suspended sediment dynamics during the inter-monsoon season in the subaqueous Mekong Delta and adjacent shelf, southern Vietnam. J. Asian Earth Sci. 79, 509–519.
Wang, L., Li, J., Lu, H., Gu, Z., Rioual, P., Hao, Q., Mackay, A.W., Jiang, W., Cai, B., Xu, B., Chu, G., 2012. The East Asian winter monsoon over the last 15,000 years: its links to high-latitudes and tropical climate systems and complex correlation to the summer monsoon. Quat. Sci. Rev. 32, 131–142.
Wijeratne, E.M.S., Pattiaratchi, C., Eliot, M., Haigh, I.D., 2012. Tidal characteristics in Bass Strait, southeast Australia. Estuar Coast Shelf Res. 114, 156–165.
Wyrtki, K., 1961. Physical oceanography of the Southeast Asian waters, Scientific Results of Marine Investigations of the South China Sea and the Gulf of Thailand 1959–1961, NAGA Rep. 2. Scripps Inst. of Oceanogr., La Jolla, California, pp. 195.
Xue, Z., He, R., Liu, J.P., Warner, J.C., 2012. Modelling transport and deposition of the Mekong river sediment. Cont. Shelf Res. 37, 66–78.
Yanagi, T., Takao, T., 1998. Clockwise phase propagation of semi diurnal tides in the Gulf of Thailand. J. Oceanogr. 54, 143–150.
Yanagi, T., Takao, T., Morimoto, A., 1997. Co-tidal and co-range charts in the South China Sea derived from satellite altimetry data.
Yao, Peng, 2015. Tidal and sediment dynamics in a fined-grained coastal region. PhD thesis. https://repository.tudelft.nl/.
Ye, A.L., Robinson, I.S., 1983. Tidal dynamics in the South China Sea. Geophys J Int 72, 691–707.
Yu, M., 1984. A preliminary study of tidal characteristics in the South China Sea. Acta Oceanol. Sin. 6, 293–300.
Zu, T., Gan, J., Erofeeva, S.Y., 2008. Numerical study of the tide and tidal dynamics in the South China Sea. Deep Sea Res. Part I Oceanogr. Res. Pap. 55, 137–154.